© 2022. Published by The Company of Biologists Ltd | Development (2022) 149, dev198341. doi:10.1242/dev.198341

RESEARCH ARTICLE

Molecular contribution to embryonic aneuploidy and karyotypic complexity in initial cleavage divisions of mammalian development

Kelsey E. Brooks[1], Brittany L. Daughtry[1,2], Brett Davis[3,4], Melissa Y. Yan[3], Suzanne S. Fei[3], Selma Shepherd[1], Lucia Carbone[4,5,6,7] and Shawn L. Chavez[1,7,8,9,*]

ABSTRACT

Embryonic aneuploidy is highly complex, often leading to developmental arrest, implantation failure or spontaneous miscarriage in both natural and assisted reproduction. Despite our knowledge of mitotic mis-segregation in somatic cells, the molecular pathways regulating chromosome fidelity during the error-prone cleavage-stage of mammalian embryogenesis remain largely undefined. Using bovine embryos and live-cell fluorescent imaging, we observed frequent micro-/multi-nucleation of mis-segregated chromosomes in initial mitotic divisions that underwent unilateral inheritance, re-fused with the primary nucleus or formed a chromatin bridge with neighboring cells. A correlation between a lack of syngamy, multipolar divisions and asymmetric genome partitioning was also revealed, and single-cell DNA-seq showed propagation of primarily non-reciprocal mitotic errors. Depletion of the mitotic checkpoint protein BUB1B (also known as BUBR1) resulted in similarly abnormal nuclear structures and cell divisions, as well as chaotic aneuploidy and dysregulation of the kinase-substrate network that mediates mitotic progression, all before zygotic genome activation. This demonstrates that embryonic micronuclei sustain multiple fates, provides an explanation for blastomeres with uniparental origins, and substantiates defective checkpoints and likely other maternally derived factors as major contributors to the karyotypic complexity afflicting mammalian preimplantation development.

KEY WORDS: Aneuploidy, BUB1B, BUBR1, Cytokinesis, Embryo, Micronuclei, Mitosis

[1]Division of Reproductive and Developmental Sciences, Oregon National Primate Research Center, Beaverton, OR 97006, USA. [2]Department of Cell, Developmental and Cancer Biology, Oregon Health and Science University, Portland, OR 97239, USA. [3]Bioinformatics and Biostatistics Unit, Oregon National Primate Research Center, Beaverton, OR 97006, USA. [4]Department of Medicine, Knight Cardiovascular Institute, Oregon Health and Science University, Portland, OR 97239, USA. [5]Division of Genetics, Oregon National Primate Research Center, Beaverton, OR 97006, USA. [6]Department of Medical Informatics and Clinical Epidemiology, Division of Bioinformatics and Computational Biomedicine, Oregon Health and Science University, Portland, OR 97239, USA. [7]Department of Molecular and Medical Genetics, Oregon Health and Science University, Portland, OR 97239, USA. [8]Department of Obstetrics and Gynecology, Oregon Health and Science University, Portland, OR 97239, USA. [9]Department of Biomedical Engineering, Oregon Health and Science University, Portland, OR 97239, USA.

*Author for correspondence (chavesh@ohsu.edu)

K.E.B., 0000-0003-3009-133X; B.L.D., 0000-0002-3526-6250; M.Y.Y., 0000-0002-8079-7923; S.S.F., 0000-0002-9688-2890; L.C., 0000-0002-2118-107X; S.L.C., 0000-0002-8285-0222

Handling Editor: Patrick Tam
Received 6 November 2020; Accepted 4 March 2022

INTRODUCTION

Multiple studies across mammalian species, including humans, have established that *in vitro*-derived embryos suffer from remarkably frequent whole-chromosomal losses and gains, or aneuploidy (Vanneste et al., 2009; Daughtry et al., 2019). Depending on the type and severity of the segregation error, many aneuploid embryos will undergo developmental arrest and/or result in early pregnancy loss if transferred. Estimates of embryonic aneuploidy *in vivo* are difficult to ascertain, but 50-70% of spontaneous miscarriages following natural conception in women are diagnosed as karyotypically abnormal (Hassold et al., 1980; Schaeffer et al., 2004). Aneuploidy can arise either meiotically during gametogenesis or post-zygotically from the mitotic cleavage divisions of preimplantation development. Although significant effort has been put forth to identify specific contributors to meiotic chromosome mis-segregation, particularly with advanced maternal age (Webster and Schuh, 2017; Schneider and Ellenberg, 2019), much less is known about the molecular mechanisms underlying mitotic aneuploidy generation. This is in spite of findings that mitotic errors are equally or more prevalent than meiotic errors, and arise independently of maternal age or fertility status (Vanneste et al., 2009; Chavez et al., 2012; McCoy et al., 2015a,b). As the first three mitotic divisions are the most error-prone and do not necessarily lead to embryo arrest at the 4- to 8-cell stage, which is when zygotic genome activation (ZGA) largely occurs in most mammals (Braude et al., 1988; Plante et al., 1994), this suggests that maternally inherited factors regulating mitotic chromosome segregation may be lacking or compromised to prevent chromosomally abnormal embryos from continuing in development (Mantikou et al., 2012; Schneider and Ellenberg, 2019; Tšuiko et al., 2019).

Our understanding of the mechanisms mediating mitotic chromosome mis-segregation primarily derives from cancer cells and tumorigenesis, and includes loss or prolonged chromosome cohesion, defective spindle attachments, abnormal centrosome number and relaxed cell cycle checkpoints (Ganem et al., 2009; Soto et al., 2019). Regardless of the mechanism, chromosomes that are mis-segregated during mitosis will become encapsulated into micronuclei and can contribute to aneuploidy in subsequent divisions. However, the cleavage divisions of preimplantation embryo development are fundamentally different from the mitoses experienced by dividing somatic cells. Besides reliance on maternally inherited signaling factors for cell division (Mantikou et al., 2012; Schneider and Ellenberg, 2019; Tšuiko et al., 2019), cleavage-stage embryos produce an increasing number of progressively smaller cells without changing the overall size of the embryo. Moreover, unlike tumors and cancer cells, which tend to express cell cycle checkpoints at high levels (Schvartzman et al., 2010), cleavage-stage human embryos have been shown to underexpress checkpoints and overexpress cell cycle drivers, at least at the RNA level (Kiessling et al., 2010). By monitoring bipolar attachment of spindle

Development (2022) 149, dev198341. doi:10.1242/dev.198341

microtubules to kinetochores during mitosis, the mitotic checkpoint complex (MCC) prevents activation of the anaphase-promoting complex/cyclosome (APC/C) and delays mitotic progression in the absence of stable bipolar kinetochore-microtubule attachments. This delay, however, is only temporary and cells with an unsatisfied checkpoint will eventually arrest or exit mitosis prematurely. The core components of the MCC are evolutionarily conserved and include CDC20, as well as the serine/threonine kinases, BUB1B, BUB3 and MAD2. Also known as BUBR1, BUB1B is the largest of the MCC proteins and is normally present throughout the cell cycle (Elowe et al., 2010). Without BUB1B/BUBR1, the MCC no longer localizes to unattached kinetochores to prevent incorrect or deficient spindle attachments, resulting in the generation of aneuploid daughter cells (Lampson and Kapoor, 2005). Whether the MCC is functional in the initial mitotic divisions of mammalian preimplantation development is currently unclear and has only been studied in mouse embryos (Wei et al., 2011; Vazquez-Diez et al., 2019), which normally exhibit a low incidence of micronucleation and aneuploidy unless treated with chemicals to inhibit MCC function (Wei et al., 2011; Bolton et al., 2016; Vazquez-Diez et al., 2019; Singla et al., 2020).

Cattle share several key characteristics of preimplantation development with humans, including the timing of the first mitotic divisions, the stage at which the major wave of ZGA occurs and the approximate percentage of embryos that typically reach the blastocyst stage (Alper et al., 2001; Wong et al., 2010; Sugimura et al., 2012). Furthermore, single-nucleotide polymorphism (SNP) genotyping and next generation sequencing (NGS) revealed that the frequency of aneuploidy in cattle is likely similar to humans (Destouni et al., 2016; Hornak et al., 2016; Tšuiko et al., 2017). Destouni et al. also demonstrated that bovine zygotes can segregate parental genomes into different blastomeres during the first cleavage division, but the mechanism by which this occurs has yet to be determined (Destouni et al., 2016). Thus, with the ethical and technical limitations of human embryo research, bovine embryos represent a suitable model for studying the dynamics of micronuclei formation and aneuploidy generation during preimplantation development. In this study, we have used a combination of time-lapse and live-cell fluorescent imaging with single-cell DNA-seq (scDNA-seq) for copy number variation (CNV) analysis to assess mitotic divisions in bovine embryos from the zygote to 12-cell stage and to visualize chromosome segregation in real-time. We also evaluated the lack of MCC function in bovine zygotes to determine whether defective cell cycle checkpoint signaling contributes to aneuploidy during early mammalian embryogenesis.

RESULTS

Abnormal nuclear structures are common in early cleavage-stage bovine embryos

Because micronuclei formation is an indication of chromosome mis-segregation, we first assessed the prevalence of micronucleation throughout bovine preimplantation development. Although micronuclei-like structures have been detected in bovine embryos previously (Yao et al., 2018), their frequency or whether they were associated with a particular stage of preimplantation development was not determined. To address this, we generated a large number (n=53) of *in vitro*-produced bovine embryos and fixed them at different stages to evaluate DNA integrity with DAPI and nuclear structure by immunostaining for the nuclear envelope marker LAMIN B1 (LMNB1; Fig. 1A). Immunofluorescent labeling revealed the presence of micronuclei as early as the zygote stage that were distinct from the maternal and paternal pronuclei (Fig. 1B). Several micronuclei, as well as multiple nuclei (multi-nuclei) of similar size, were also detected at the early cleavage stage (Fig. 1C). Overall, 37.7% (n=20/53) of early cleavage-stage embryos exhibited micro-/multi-nucleation in one or more blastomeres, suggesting that their formation before ZGA is conserved between cattle and primates (Chavez et al., 2012; Daughtry et al., 2019). A similar examination of bovine blastocysts also immunostained for the trophoblast marker caudal type homeobox 2 (CDX2) demonstrated that micronuclei often reside in the trophectoderm (TE; Fig. 1D), but can also be contained within the inner cell mass (ICM) of the embryo (Fig. 1E). In order to confirm these findings, we immunostained bovine blastocysts using using an antibody to annexin A2 (ANXA2), a membrane-associated adhesion molecule important for embryo attachment and trophoblast outgrowth (Garrido-Gómez et al., 2012; Wang and Shao, 2020) that is highly expressed in early trophoblasts (Fig. S1A,B), and showed the retention of ANXA2-negative micronuclei in the ICM (Fig. S1C-E). However, it is also possible that these micronuclei were not fully integrated into the ICM and instead were produced from apoptosis, which is known to occur in this compartment of *in vitro*-derived bovine blastocysts (Gjorret et al., 2003).

Live-cell fluorescent imaging reveals micronuclei fate and the potential origin of uniparental cells

To visualize the formation of micro- and multi-nuclei in real-time and determine the fate of these nuclear structures in subsequent divisions, we microinjected bovine zygotes (n=90) with fluorescently labeled modified mRNAs and monitored the first three mitoses by live-cell confocal microscopy (Fig. 1A). Histone H2B and/or LMNB1 were used to visualize DNA and nuclear envelope, respectively, whereas F-actin was able to distinguish blastomeres (Movie 1). Of the microinjected embryos, 18.9% (n=17/90) failed to complete cytokinesis during microscopic evaluation, while 53.3% (n=49/90) exhibited normal bipolar divisions and 27.8% (n=25/90) underwent multipolar divisions from one cell to three cells or more (Fig. 2A). In accordance with our immunostaining findings, 31.1% (n=28/90) of the embryos contained micro- and/or multi-nuclei, and anaphase lagging of chromosomes was detected before their formation in only three of these embryos at the zygote (Fig. 2B) or two-cell (Fig. 2C) stage. Micro- and multi-nucleation was more frequently associated with bipolar divisions (Fig. 2A) and an examination of micronuclei fate demonstrated an equal incidence of unilateral inheritance (Fig. 2D) or re-fusion with the primary nucleus (Fig. 2E), while a smaller percentage appeared to form a chromatin bridge with a neighboring blastomere (Fig. 2F, Fig. S2 and Movie 1). Interestingly, the majority of multipolar embryos (76%; n=19/25) underwent the abnormal division after bypassing the fusion of maternal and paternal pronuclei that is known as syngamy (Fig. 2G), and/or produced daughter cells that did not contain any apparent nuclear structure (Fig. 2H). These results help explain previous findings of blastomeres with uniparental origins and those that completely lacked nuclear DNA when assessed for CNV, respectively (Destouni et al., 2016; Ottolini et al., 2017; Daughtry et al., 2019; Middelkamp et al., 2020).

Non-reciprocal mitotic errors are highly prevalent in early cleavage divisions

Given the large aneuploidy range reported (32-85%) and differences in the embryonic stage, proportion of the embryo analyzed or CNV approach used in previous bovine studies (Destouni et al., 2016;

Development (2022) 149, dev198341. doi:10.1242/dev.198341

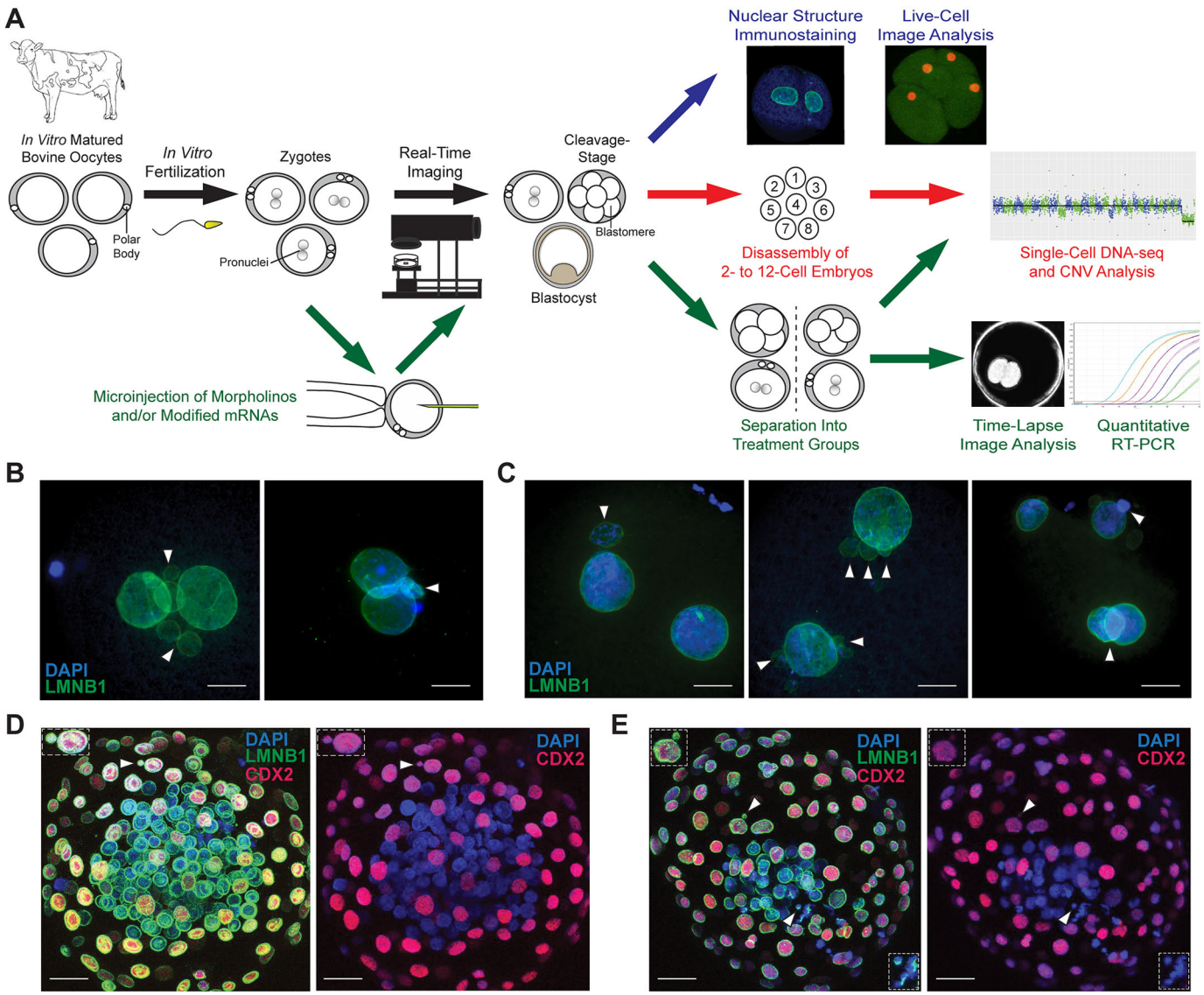

Fig. 1. Investigating the dynamics of mitotic chromosome segregation and MCC fidelity in bovine embryos. (A) *In vitro*-produced bovine oocytes underwent IVF and the resulting zygotes were non-invasively monitored by time-lapse image analysis until collection for immunostaining of nuclear structure (n=53). Another subset of zygotes was microinjected with fluorescently labeled modified mRNAs and chromosome segregation visualized during the first three mitotic divisions in real-time by live-cell confocal microscopy (n=90). Embryos were disassembled into single blastomeres at the 2- to 12-cell stage for scDNA-seq and CNV analysis to determine the precise frequency of aneuploidy at the early cleavage stages (n=38). Other zygotes were microinjected with non-overlapping morpholinos targeting the mitotic checkpoint protein BUB1B and/or modified BUB1B mRNA to test the effect and specificity of MCC inhibition on chromosome segregation, division dynamics and preimplantation development (n=430). Gene expression profiling was also conducted on a subset of MCC-deficient zygotes versus controls by quantitative RT-PCR to identify changes in gene abundance and molecular pathways associated with BUB1B knockdown (n=15). (B,C) Immunostaining of zygotes (B) and cleavage-stage embryos (C) with LMNB1 (green) using DAPI (blue) to visualize DNA revealed several micro- and multi-nuclei (white arrowheads). (D,E) Blastocysts also immunostained for the trophoblast marker CDX2 (red) showed that micronuclei (arrowheads) are often present in the TE (E), but can also be retained within the ICM of the embryo. In D, the micronucleus is present in the TE; in E, micronuclei are present in both the TE (top left) and the ICM (bottom right). Scale bars: 10 µm.

Hornak et al., 2016; Tšuiko et al., 2017), we sought to determine the precise frequency of aneuploidy in a large number of bovine embryos (n=38) at the early cleavage stages using high-resolution scDNA-seq (Fig. 1A and Table S1). Each embryo was disassembled into individual blastomeres and all cells were assessed to ensure an accurate representation of the overall embryo, resulting in the analysis of 133 blastomeres from the 2- to 12-cell stage (Fig. 3A). Based on previously described criteria (Daughtry et al., 2019), we classified 25.6% (n=34/133) of the blastomeres as euploid and 35.3% (n=47/133) as aneuploid; 3% (n=4/133) solely contained segmental errors and 17.3% (n=23/133) exhibited chaotic aneuploidy. The remaining cells either failed WGA (10.5%; n=14/133) or were identified as empty due to the detection of only mitochondrial DNA (8.3%; n=11/133). After combining the results from each embryo, we determined that 16% (n=6/38) were entirely euploid, whereas 55% (n=21/38) comprised only aneuploid cells (Fig. 3B). An additional 29% (n=11/38) contained a combination of both euploid and aneuploid blastomeres, known as mosaic. Of the embryos with mosaicism, 18% (n=2/11) had incurred segmental errors only or DNA breaks of 15 Mb in length or larger that did not affect the whole chromosome. Whole-chromosomal losses (58.4%) were more prevalent than

Development (2022) 149, dev198341. doi:10.1242/dev.198341

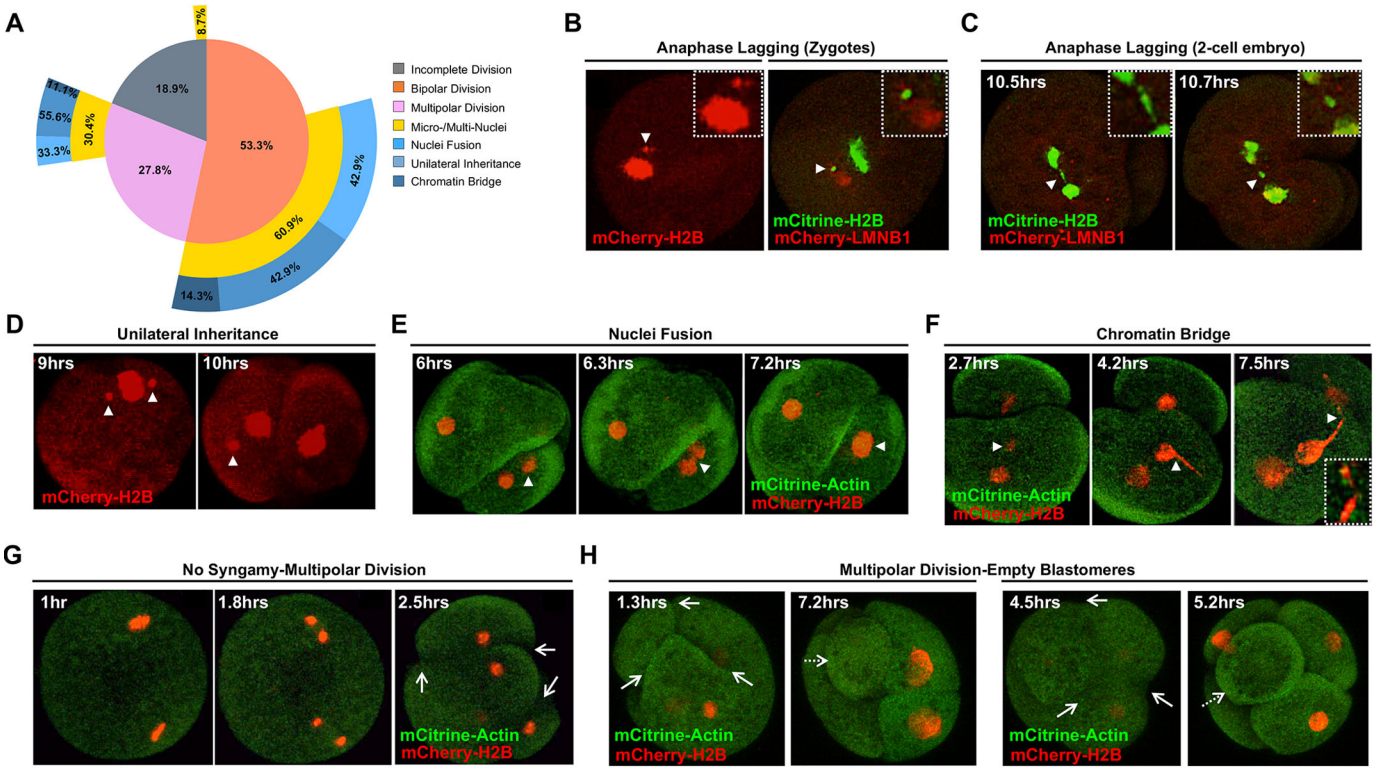

Fig. 2. Live-cell fluorescent imaging reveals micronuclei fate and uniparental genome distribution to daughter cells. Bovine zygotes were microinjected with fluorescently labeled modified mRNAs (mCitrine or mCherry) to visualize DNA (Histone H2B) or nuclear structure (LMNB1) and distinguish blastomeres (F-actin) by live-cell confocal microscopy during the first three mitotic divisions (n=90). (A) A Venn Pie that shows the percentage of embryos that did not complete cytokinesis (gray), exhibited normal bipolar divisions (orange) or underwent multipolar divisions at the zygote or two-cell stage (pink). The percentage of embryos with micro- and/or multi-nuclei (MN; yellow) associated with each type of division is also shown. Micronuclei fate is represented as those that formed a chromatin bridge (dark blue), exhibited unilateral inheritance (medium blue) or re-fused with the primary nucleus (light blue). Most embryos underwent bipolar divisions and were more likely to contain micronuclei than multipolar embryos. (B,C) Anaphase lagging of chromosomes (white arrowheads) was detected in certain embryos at the zygote (B) or two-cell (C) stage before micronuclei formation. (D-F) An examination of micronuclei fate demonstrated that relatively equal proportions persist and undergo unilateral inheritance (D) or fuse back with the primary nucleus (E), with a small number exhibiting what appeared to be a chromatin bridge between blastomeres following micronuclei formation (F) (white arrowheads). (G,H) The majority of multipolar embryos (white solid arrows) bypassed pronuclear fusion (syngamy) before the abnormal division (G) and often produced blastomeres with asymmetric genome partitioning and/or no apparent nuclear structure (H, white dashed arrows). Numbers in the top left corner indicate the time since the start of imaging; the auto-labeling of each embryo used for identification and/or tracking purposes has been masked for clarity where necessary.

whole-chromosomal gains (41.6%), while segmental losses and gains were equally prevalent. The X chromosome was by far the most frequently impacted by whole chromosomal losses and gains, whereas chromosome 5 (human chromosomes 12 and 22), 7 (human chromosomes 5 and 19), 11 (human chromosomes 3 and 9) and 29 (human chromosome 11) were commonly subjected to DNA breakage (Fig. 3C). Although meiotic mis-segregation was identified in 16% (n=6/38) of the embryos (Fig. 3D), mitotic aneuploidy accounted for the majority of errors (66%; n=25/38), with the remaining 18% (n=7/38) exhibiting the karyotypic complexity characteristic of chaotic aneuploidy (Fig. 3E). In addition, most (67%; n=4/6) of the embryos with meiotic errors also experienced mitotic mis-segregation of different chromosomes than those originally affected during meiosis (Fig. 3F). Reciprocal losses and gains, whereby chromosomes lost from one blastomere were found in a sister blastomere, accounted for only 25% (n=7/29) of the mitotic errors (Fig. 3D,F).

Assessment of BUB1B knockdown efficiency in bovine cells and embryos

Since this chromosome constitution indicated deficient cell cycle checkpoints and there are conflicting reports on whether the MCC is functional at the early cleavage stage in mice (Wei et al., 2011; Vazquez-Diez et al., 2019), our next objective was to determine whether a lack of adequate checkpoints was associated with micro-/multi-nucleation and aneuploidy in bovine embryos (Fig. 1A). Given negligible effects on mouse embryogenesis from knockdown of Mad2, another MCC component (Vazquez-Diez et al., 2019), we focused our attention on BUB1B (also known as BUBR1), the largest of the MCC proteins that is present throughout the cell cycle (Elowe et al., 2010). Two non-overlapping morpholino antisense oligonucleotides (MAOs) were designed to specifically inhibit BUB1B by targeting the ATG translation start site (BUB1B MAO 1) or a sequence upstream within the 5′ UTR (BUB1B MAO 2) and tested before use in embryos (Fig. S3A). Because BUB1B is diffusely expressed in the cytoplasm of cells in interphase and only concentrates at kinetochores in early prophase (Simmons et al., 2019), the visualization of BUB1B expression and localization requires that all cells be undergoing mitosis. However, blastomeres in early cleavage-stage mammalian embryos exhibit asynchronous cell division rather than simultaneously dividing like in other vertebrates (Gilbert, 2000), and the addition of chemicals such as colcemid to arrest cells in metaphase can induce aneuploidy by themselves (Held, 1982; Ligasová and Koberna, 2021). Therefore, we used the Madin-Darby Bovine Kidney (MDBK) epithelial cell line to assess BUB1B expression in non-transfected

Development (2022) 149, dev198341. doi:10.1242/dev.198341

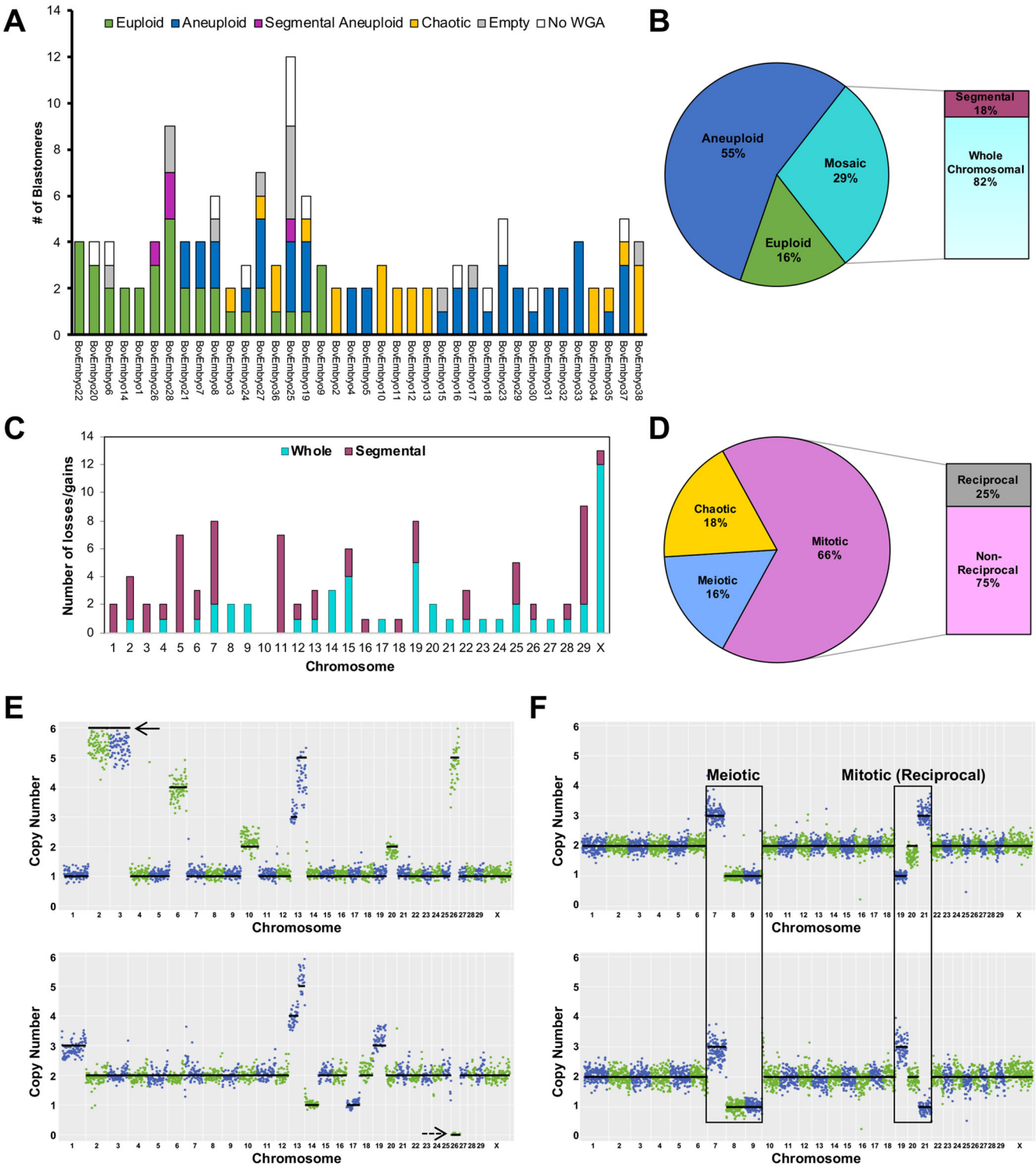

Fig. 3. Comprehensive assessment of chromosomal abnormalities in early cleavage-stage embryos by scDNA-seq. (A) Whole-chromosome and sub-chromosomal CNV was evaluated in bovine embryos from the 2- to 12-cell stage (*n*=38). Stacked bars represent all blastomeres (*n*=133) classified as euploid (green), aneuploid (blue), segmental aneuploid (purple), chaotic aneuploid (yellow), empty (gray) or failing to undergo WGA (white). (B) Pie chart showing the overall chromosome status of the embryos. (C) Number of whole or segmental chromosome losses and/or gains affecting each chromosome. There is frequent mis-segregation of the X-chromosome and DNA breakage in chromosomes 5, 7, 11 and 29. (D) The percentage of aneuploid embryos with each type of chromosomal error. (E) CNV plots of blastomeres from two different embryos with chaotic aneuploidy showing up to six copies of some chromosomes (top; black solid arrow) and a complete loss of other chromosomes (bottom; black dashed arrow). (F) Blastomeres from a two-cell embryo with meiotic errors (chromosomes 7, 8 and 9) propagated during the first cleavage division that also experienced mitotic mis-segregation of different chromosomes (chromosomes 19 and 21) that were reciprocal.

Development (2022) 149, dev198341. doi:10.1242/dev.198341

cells for comparison to those transfected with either a standard control (Std Control) MAO or BUB1B MAO 1 and observed a reduction in BUB1B expression only in the latter by immunofluorescence (Fig. S3B). Quantification of the percentage of MDBK cells with positive BUB1B expression following transfection with different concentrations of each MAO revealed a dose-dependent decrease in BUB1B expression in BUB1B MAO 1 transfected cells (Fig. S3C). This was further assessed by western blot analysis of MDBK cells treated with or without colcemid prior to mitotic shake-off, which takes advantage of cells detaching from the culture substrate and rounding up during mitosis (Ligasová and Koberna, 2021), and showed reduced BUB1B expression following colcemid treatment (Fig. S3D). To determine whether BUB1B knockdown was similarly efficient in embryos, bovine zygotes were microinjected with the Std Control MAO (n=5) or BUB1B MAO 1 (n=5), and BUB1B expression was evaluated by microfluidic quantitative RT-PCR (RT-qPCR). As shown in Fig. S3E, we detected a significant (P=0.007) decrease in BUB1B expression in the BUB1B MAO-injected embryos compared with those injected with the Std Control MAO.

MCC deficiency induces atypical cytokinesis, blastomere asymmetry and developmental arrest

Once we confirmed BUB1B knockdown efficiency, bovine zygotes were microinjected with either Std Control MAO (n=81), BUB1B MAO 1 (n=48) or BUB1B MAO 2 (n=36) and cultured under a time-lapse imaging microscope to monitor development. Each embryo was categorized as having either normal or abnormal divisions for comparison with untreated (non-injected) embryos (n=180). In the BUB1B MAO 1 treatment group, 37.5% (n=18/48) of the zygotes failed to undergo the first cleavage division (Table 1) and a subset (8.3%; n=4/48) of these embryos attempted to divide by forming multiple cleavage furrows (Fig. 4A), but never successfully completed cytokinesis (Movie 2). Of those BUB1B MAO 1 zygotes that divided, more exhibited abnormal cytokinesis (65.4%; n=17/26), including multipolar divisions and/or blastomere asymmetry (Movies 3 and 4, respectively), than normal bipolar divisions (30%; n=9/30). Similar results were obtained following injection with BUB1B MAO 2 (Table 1 and Fig. 4B); despite the phenotypic similarities between the two non-overlapping MAOs, we further assessed BUB1B MAO specificity by conducting embryo rescue experiments with modified BUB1B mRNA that would not be directly targeted by the MAO. BUB1B mRNA with a mutated MAO-binding sequence was microinjected into zygotes, along with BUB1B MAO 1 (n=51), and embryos cultured up to the blastocyst stage (Fig. 4C). Although no embryos formed blastocysts following injection of either the BUB1B MAO 1 or 2, 45% (n=23/51) of the BUB1B MAO 1 and mRNA co-injected embryos underwent cleavage divisions and reached the blastocyst stage (Fig. 4D). This percentage was similar to that obtained from the non-injected embryos and following injection with the Std Control MAO, confirming that the knockdown of BUB1B expression and rescue of BUB1B-induced mitotic defects were specific.

MCC-deficient embryos exhibit micro-/multi-nucleation and asymmetric genome distribution

Because none of the BUB1B MAO-injected embryos formed blastocysts and instead arrested at the early cleavage stage, we next examined nuclear structure and CNV in MCC-deficient embryos by immunofluorescence and scDNA-seq, respectively (Fig. 1A). LMNB1 immunostaining revealed both micro- and multi-nuclei in BUB1B MAO 1- and 2-treated embryos that did not attempt division or were unable to complete the first cytokinesis (Fig. 4E, top row). Similar abnormal nuclear structures, as well as empty blastomeres or those with DNA that lacked a nuclear envelope, were also apparent in MCC-deficient embryos that successfully divided (Fig. 4E, bottom row). Disassembly of the embryos into individual cells for assessment of DNA content and CNV analysis demonstrated that, while euploid blastomeres could be obtained following BUB1B MAO injection, MCC deficiency mostly produced blastomeres with chaotic aneuploidy (Fig. 4F). Analogous to some of the non-injected controls (Fig. 3E), a complete loss of certain chromosomes and a gain of up to six copies of other chromosomes were detected, suggesting that the lack of MCC function permits premature mitotic exit, micro-/multi-nucleation and asymmetrical genome distribution upon division.

MCC deficiency at the first division impacts cell cycle progression and kinase network activity

Based on findings that several BUB1B-deficient embryos did not divide or exhibited abnormal multipolar and/or asymmetric divisions, we sought to determine whether BUB1B knockdown had specific effects on the mitotic machinery or whether it induced a broader dysregulation of mitosis. Therefore, the relative abundance of additional maternal-effect, mitotic, cell cycle, ZGA and cell survival genes was assessed in individual BUB1B MAO 1 versus non-injected and Std Control-injected MAO zygotes (Fig. S3 and Table S2) using microfluidic RT-qPCR. Besides BUB1B (Fig. S3E), the genes encoding several other kinases involved in cytokinesis and chromosome segregation, including aurora kinase B (*AURKB*), Polo-like kinase 1 (*PLK1*) and ribosomal protein S6 kinase alpha-5 (*RPS6KA5*), were all significantly downregulated in BUB1B MAO-injected embryos relative to the controls (Fig. 5A; $P \leq 0.05$). Expression of additional genes, including amyloid β precursor protein binding family B member 1 (*APBB1*), which inhibits cell cycle progression, and those associated with extracellular matrix remodeling [cartilage acidic protein 1 (*CRTAC1*) and ADAM metallopeptidase with thrombospondin type 1 motif 2 (*ADAMTS2*)] and the stress response (endoplasmic

Table 1. Division dynamics in untreated embryos and MAO treatment groups

	Untreated (non-injected)	Standard control MAO	BUB1B MAO 1	BUB1B MAO 2
No division	8.3% (n=15/180)	24.7% (n=20/81)	37.5% (n=18/48)	33.3% (n=12/36)
Attempted division	10% (n=18/180)	2.5% (n=2/81)	8.3% (n=4/48)	0.0% (n=0/36)
Normal bipolar/symmetric division	72.8% (n=107/147)	62.7% (n=37/59)	34.6% (n=9/26)	25.0% (n=6/24)
Abnormal multipolar/asymmetric division	27.2% (n=40/147)	37.3% (n=22/59)	65.4% (n=17/26)	75.0% (n=18/24)
Total number of embryos	180	81	48	36

Summary of the percentage of bovine zygotes that exhibited no division or attempted to divide as well as those that had normal bipolar/symmetric versus abnormal multipolar/asymmetric divisions following no treatment or microinjection with standard control, BUB1B MAO 1 or BUB1B MAO 2. Attempted division was defined by the identification of cleavage furrows without the completion of cytokinesis. In contrast to the controls, BUB1B MAO 1- and BUB1B MAO 2-injected embryos were more likely to undergo multipolar and/or asymmetric divisions.

Development (2022) 149, dev198341. doi:10.1242/dev.198341

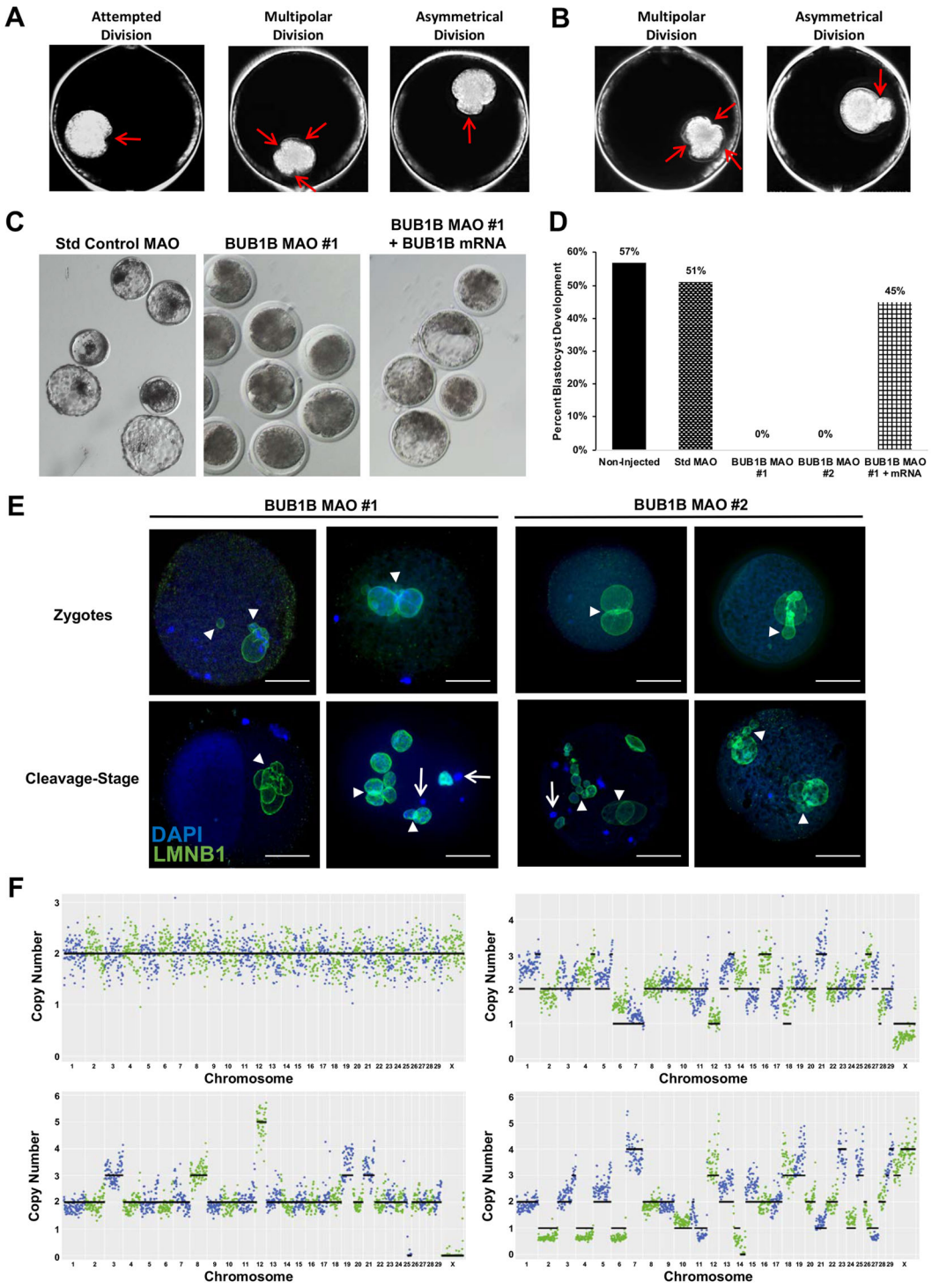

Fig. 4. BUB1B knockdown induces multipolar divisions, chaotic aneuploidy and developmental arrest. (A,B) Darkfield time-lapse imaging frames depicting the various embryo phenotypes (red arrows), including attempted division, multipolar division and blastomere asymmetry observed following BUB1B MAO 1 (A) or BUB1B MAO 2 (B) microinjection in bovine zygotes. (C) Representative stereomicroscope images of embryos and blastocysts from the Std Control MAO, BUB1B MAO 1, and BUB1B MAO 1 and BUB1B modified mRNA treatment groups. (D) Bar graph of the percentage of embryos that reached the blastocyst stage in non-injected (n=180), Std Control MAO- (n=81), BUB1B MAO 1- (n=48), BUB1B MAO 2- (n=36), or BUB1B MAO 1- and BUB1B modified mRNA-injected zygotes (n=85). Although no blastocysts were obtained following BUB1B MAO 1 or 2 treatment, the co-injection of BUB1 MAO 1 and BUB1B modified mRNA was able to almost fully rescue the phenotype and restore blastocyst formation rates to that observed in controls. (E) Confocal images of LMNB1 (green) immunostaining in BUB1B MAO 1- or 2-treated embryos stained with DAPI (blue). Abnormal nuclear morphology and the presence of both micro- and multi-nuclei were detected (white arrowheads) in embryos at the zygote stage (top row) and cleavage stage that exhibited abnormal cell divisions (bottom row). DNA without a nuclear envelope (white arrows) and a blastomere that completely lacked nuclear material are present in the two-cell embryo located in the lower-left image. Scale bars: 10 µm. (F) CNV plots of blastomeres from different cleavage-stage embryos disassembled into single cells following BUB1B 1 MAO injection. Although some euploid blastomeres were detected in BUB1B-injected embryos (upper left plot), most exhibited chaotic aneuploidy with multiple whole and sub-chromosomal losses and gains.

Development (2022) 149, dev198341. doi:10.1242/dev.198341

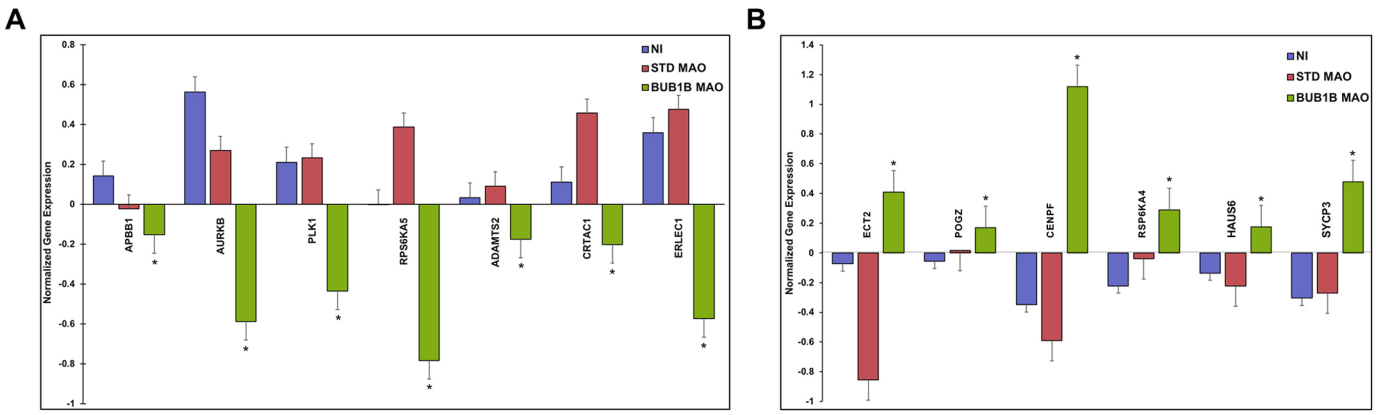

Fig. 5. BUB1B deficiency in zygotes primarily impacts the expression of other protein kinases and kinase substrates. The relative abundance of several mitotic, cell cycle, developmentally regulated and cell survival genes was assessed via microfluidic quantitative RT-PCR (RT-qPCR) in non-injected (NI; *n*=5), Std Control MAO-treated (*n*=5) and BUB1B MAO 1-treated (*n*=5) individual zygotes using gene-specific primers. (A) The genes that were significantly downregulated (*$P \leq 0.05$) in BUB1B MAO-injected embryos compared with the NI and Std Control MAO are shown in the bar graph (data are mean±s.e.m.). (B) A bar graph of the genes that were significantly upregulated (*$P \leq 0.05$) in BUB1B MAO-injected embryos relative to the controls (data are mean±s.e.m.). Mean CNRQ values for each gene were compared across embryo groups using the Mann–Whitney *U*-test. The full list of the 96 genes and primer sequences assessed by RT-qPCR is available in Fig. S4 and Table S2, respectively.

reticulum lectin 1; *ERLEC1*) was also significantly decreased in MCC-deficient embryos. In contrast, genes involved in promoting cell cycle progression, such as epithelial cell transforming 2 (*ECT2*), pogo transposable element derived with ZNF domain (*POGZ*), centromere protein F (*CENPF*) and ribosomal protein S6 kinase alpha 4 (*RPS6KA4*), were significantly upregulated in BUB1B MAO-injected embryos, along with microtubule polymerization (HAUS augmin like complex subunit 6; *HAUS6*) or orientation (synaptonemal complex protein 3; *SYCP3*) genes (Fig. 5B; $P \leq 0.05$). Because ECT2, POGZ, CENP-F, HAUS6 and SYCP3 have been shown to serve as kinase substrates in dividing somatic cells (Kettenbach et al., 2011; Santamaria et al., 2011; Bibi et al., 2013), this suggests that the inhibition of BUB1B primarily increases the phosphorylation and expression of kinase substrates either directly or indirectly via regulation by other protein kinases, such as AURKB, PLK1 and RPS6KA5.

DISCUSSION

Aneuploidy is a major cause of embryo arrest, implantation failure and spontaneous miscarriage during mammalian development, and, yet, relatively little is still known about the molecular mechanism(s) mediating mitotic chromosome mis-segregation. Because mitotic errors can be as detrimental as meiotic errors or produce chromosomally mosaic embryos that continue in development and still implant (Magli et al., 2000; Baltaci et al., 2006; Fragouli et al., 2014, 2017; Greco et al., 2015), it is imperative that we identify euploid and mosaic embryos with high implantation potential before they are transferred. Although there are multiple mechanisms that could mediate mitotic chromosome mis-segregation, within the context of preimplantation development, only the MCC has been examined and these studies primarily used mouse embryos treated with chemicals to induce aneuploidy (Wei et al., 2011; Bolton et al., 2016; Vazquez-Diez et al., 2019). In addition, the knockdown of a specific MCC component in mouse zygotes had no effect on the first cleavage divisions when mitotic aneuploidy typically occurs in other mammals (Vazquez-Diez et al., 2019), questioning whether the MCC is functional in early mammalian embryos. Using a combination of live-cell imaging, scDNA-seq, immunofluorescence and genetic manipulation, we visualized mitotic chromosome segregation in real-time from the zygote to the 12-cell stage and assessed the role of the MCC in embryos from an animal model that suffers from a comparable incidence of aneuploidy to that in humans.

Of the cleavage-stage embryos examined by immunostaining or live-cell imaging, over 30% contained micro- or multi-nuclei, and anaphase lagging of chromosomes was detected in a small number of embryos prior to micronuclei formation. When we evaluated other morphological or mitotic characteristics that might indicate how these abnormal nuclear structures formed, we determined that most micronuclei-containing embryos underwent normal bipolar divisions, excluding multipolar cytokinesis as the primary mechanism. However, multipolar divisions were associated with a lack of syngamy and often produced cells that did not contain any apparent nuclear structure (Fig. 6A). Whereas mouse zygotes have been shown to sustain spatial separation of parental genomes by dual-spindle formation (Mayer et al., 2000; Reichmann et al., 2018), embryos from other mammals, including humans, are thought to exhibit syngamy at the zygote stage (Kai et al., 2018; Yao et al., 2018). However, recent studies with both bovine and human embryos showed that the clustering and unification of parental genomes often fails, resulting in micronuclei formation and chromosome mis-segregation (Cavazza et al., 2021), and dual-spindle formation can occur in bovine zygotes despite the presence of paternal centrosomes (Schneider et al., 2021). By avoiding syngamy and then undergoing abnormal cytokinesis, zygotes could differentially segregate entire parental genomes to daughter cells, which has been termed ‘heterogonic division’ (Destouni et al., 2016). Although we were unable to confirm that these embryos underwent heterogonic divisions by SNP analysis due to the lack of maternal DNA input available from all oocyte donors, our findings provide a mechanism for how blastomeres with uniparental origins could arise in both cattle and primates. It may also help explain the potential higher risk of uniparental disomy disorders such as Angelman syndrome and Prader-Willi syndrome in human embryos derived *in vitro* (Gosden et al., 2003; Hattori et al., 2019). Based on the prevalence of blastomeres with uniparental origins reported in these studies (Destouni et al., 2016; Ottolini et al., 2017; Daughtry et al., 2019; Middelkamp et al., 2020), we suggest that SNP-based

Development (2022) 149, dev198341. doi:10.1242/dev.198341

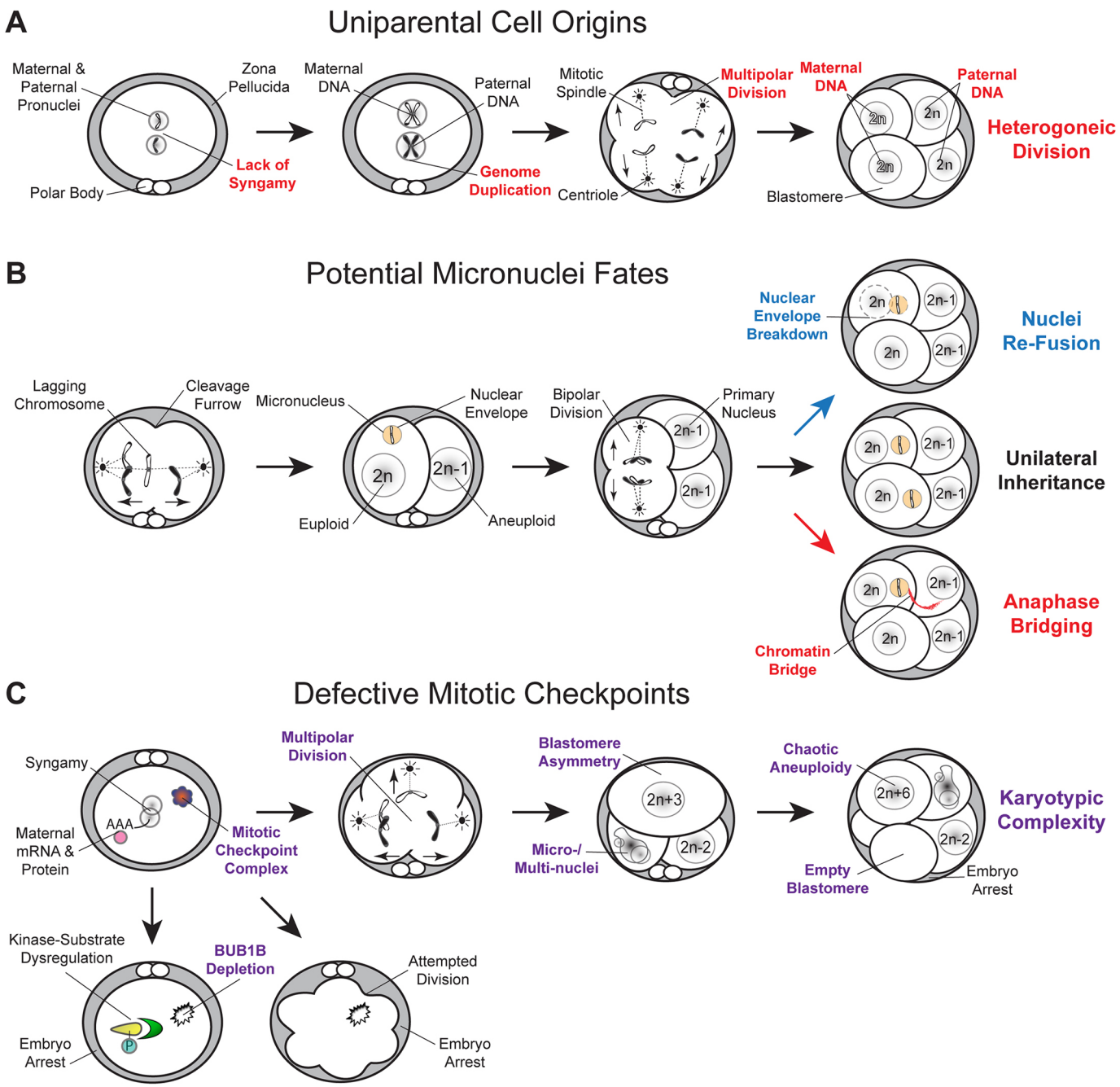

Fig. 6. Summary of the major conclusions from the imaging, scDNA-seq and gene knockdown studies. (A) Simplified model of how the lack of maternal and paternal pronuclear fusion (syngamy) at the zygote stage, followed by genome duplication and multipolar divisions, could contribute to blastomeres with uniparental origins or to those that contain only maternal or paternal DNA. (B) Live-cell imaging also revealed the formation of anaphase lagging chromosomes likely from merotelic attachments before or during the first mitotic division. The chromosome(s) become encapsulated in nuclear envelope to form a micronucleus and the embryo continues to divide normally. In these subsequent bipolar divisions, most micronuclei either fuse back with the primary nucleus upon nuclear envelope breakdown or persist and undergo unilateral inheritance; however, some micronuclei form a chromatin bridge with the nucleus of another blastomere during anaphase. (C) The depletion of BUB1B in zygotes resulted in no division or attempted division and in embryo arrest, while multipolar divisions, blastomere asymmetry and micro-/multi-nuclei were observed in MCC-deficient embryos that completed the first cytokinesis. These abnormal divisions also produced daughter cells with chaotic aneuploidy and/or empty blastomeres with no nuclear structure that induced embryo arrest, which suggested that the lack of MCC permits the karyotypic complexity detected at the early cleavage-stages of preimplantation development.

strategies should be used to accurately assess embryo ploidy and distinguish the parental source of all DNA, as it may reveal why some seemingly ‘euploid’ embryos fail to implant.

Examination of micronuclei fate in subsequent divisions revealed an equal incidence of unilateral inheritance and fusion back with the primary nucleus, with a smaller percentage of embryos exhibiting a chromatin bridge between blastomeres following micronucleation (Fig. 6B). Because cancer cell micronuclei have been shown to undergo extensive DNA damage upon re-fusion with the primary nucleus (Crasta et al., 2012; Zhang et al., 2015), chromosomal integrity and the effect on developmental outcome will likely differ depending on which of these events occurred. The significance of

Development (2022) 149, dev198341. doi:10.1242/dev.198341

the chromatin bridging and whether it exacerbates aneuploidy or restores euploidy is currently unknown, but we suspect that this genetic exchange between blastomeres contributes to the high frequency of non-reciprocal mitotic errors observed here and in embryos from other mammals (Vanneste et al., 2009; Chavez et al., 2012; McCoy et al., 2015a; Daughtry et al., 2019). A similar assessment of bovine blastocysts determined that micronuclei can reside in both the placental-derived TE and ICM of the embryo, the latter of which may be more detrimental. It is estimated that 40% of human blastocysts are aneuploid to some extent (Fiorentino et al., 2014; Popovic et al., 2018) and a recent study suggests that 24% of bovine blastocysts are aneuploid, with a high degree of concordance in the incidence of aneuploidy between the TE and ICM lineages (Tutt et al., 2021). However, these percentages are based on the assessment of multiple cells together rather than at the single-cell level, making it difficult to determine the extent of chromosomal mosaicism in an embryo. Using single-cell RNA-seq (scRNA-seq) data to infer chromosome dosage from gene expression differences (Petropoulos et al., 2016; Griffiths et al., 2017), a recent study observed no significant enrichment of aneuploid cells in the TE compared with ICM of human blastocysts, but only 31 ICM cells from 23 embryos was examined (Starostik et al., 2020). Nevertheless, the authors also reported that 31% of the embryos possessed meiotic aneuploidies, while mitotic aneuploidies were detected in 74% of the embryos. This suggests that mitotic errors are more likely to be observed in blastocysts, where they may be more tolerated than meiotic errors, and until aneuploidy is comprehensively examined at the single-cell level in whole blastocysts, the precise distribution of aneuploid cells between the TE and ICM will remain unclear.

Although SNP arrays and NGS have been used previously to assess aneuploidy in cleavage-stage bovine embryos, these studies reported a large aneuploidy range, examined a single stage of development and/or evaluated only part of the embryo (Destouni et al., 2016; Hornak et al., 2016; Tšuiko et al., 2017). After karyotypically reconstructing each embryo and combining the scDNA-seq results, we determined that over half the embryos contained only aneuploid cells. One-third of the remaining embryos were chromosomally mosaic, all of which were primarily the product of non-reciprocal mitotic errors. In those embryos with meiotic errors, most also experienced mitotic mis-segregation of different chromosomes than those originally affected during meiosis, indicating that embryos with meiotic errors are more prone to additional mitotic mis-segregation events that are further propagated during subsequent divisions. The rest of the aneuploid embryos exhibited a compete loss and/or a gain of up to six copies of chromosomes characteristic of chaotic aneuploidy from multipolar divisions (Ottolini et al., 2017; Daughtry et al., 2019). A previous study comparing *in vivo* ovulated (IVO) versus *in vitro* matured (IVM) mouse oocytes showed that the aneuploidy frequency in embryos produced with IVO oocytes increased from 3.7% to 9.4% with IVM oocytes (Treff et al., 2016). These percentages were exacerbated by advanced maternal age, increasing from 12.8% in embryos generated with IVO oocytes to 30.8% with IVM oocytes, and suggesting that older oocytes are more susceptible to aneuploidy regardless of whether derived *in vivo* or *in vitro*. Because the bovine oocytes used in this study were obtained from young females, we expect that IVM had less impact on the incidence of aneuploidy than if the oocytes were collected from older female donors. Nonetheless, it should be noted that IVM of oocytes can increase aneuploidy by itself, although not likely to the levels observed in this study given the relatively low frequency of meiotic errors.

Because of the discrepancy in whether the MCC is functional in the early cleavage divisions of mouse embryogenesis in previous studies (Wei et al., 2011; Vazquez-Diez et al., 2019), we investigated the consequences of MCC inhibition by targeting BUB1B in bovine zygotes. Following injection, BUB1B MAO embryos either failed to divide even after several attempts or exhibited abnormal divisions that were multipolar and/or asymmetrical (Fig. 6C). Furthermore, immunostaining of the BUB1B MAO-treated embryos that did divide revealed blastomeres with abnormal nuclear structures or completely devoid of nuclear DNA. CNV analysis of blastomeres that contained DNA showed a predominance of chaotic aneuploidy, with a complete loss or excessive number of chromosomal copies as described in some untreated embryos here and previously reported in primate embryos with multipolar divisions (Ottolini et al., 2017; Daughtry et al., 2019). Without BUB1B, we speculate that embryos were unable to obtain proper microtubule-kinetochore attachments prior to the first cytokinesis, resulting in failed MCC and arrest, or underwent premature cell division and chromosome mis-segregation due to MCC dysregulation. Although knockdown of another MCC component, Mad2, in mouse embryos was recently shown to have no effect on blastocyst formation, it did increase the number of micronuclei present at the morula stage (Vazquez-Diez et al., 2019). Both MAD2 and BUB1B bind CDC20 to prevent activation of the APC, but *in vitro* binding assays demonstrate that BUB1B is 12 times more effective than MAD2 in inhibiting CDC20 (Fang, 2002). In addition, it has been shown in *Drosophila* that the recruitment of Cdc20 to the kinetochore requires Bub1b and not Mad2 (Li et al., 2010). Based on these findings and the observation that BUB1B differs from the other MCC components in that both underexpression and overexpression result in drastically different phenotypes, including infertility in hypomorphic *Bub1b* mice (Baker et al., 2004, 2013), we postulate that BUB1B is the foremost checkpoint regulator. Moreover, as *BUB1B* mRNA is highly expressed in oocytes and has been shown to be a maternal effect gene (Pérez-Mongiovi et al., 2005; Gasca et al., 2007), we suspect that it mainly ensures chromosome fidelity during the error-prone early cleavage divisions, but an embryonic form of BUB1B expressed upon ZGA may also serve a role later in preimplantation development.

Given that many BUB1B-deficient embryos attempted to divide, but did not complete cytokinesis, or exhibited abnormal divisions, we evaluated whether BUB1B abundance affected the expression of other maternal-effect, mitotic, cell cycle, ZGA or cell survival genes. Although some genes involved in extracellular matrix remodeling and the stress response were impacted by BUB1B deficiency, the primary effect of BUB1B knockdown was the downregulation of the protein kinases *AURKB*, *PLK1* and *RPS6KA5*, and the upregulation of several kinase substrates. Another protein kinase, *RPS6KA4*, that we have shown is associated with binucleation, mitotic arrest and blastomere lysis in mouse embryos, as well as aneuploidy in human embryos, was significantly upregulated in BUB1B-deficient embryos (Chavez et al., 2014). In somatic cells, BUB1B requires PLK1 to function (Elowe et al., 2007) and together they inhibit kinase activity at kinetochores through positive feedback (Suijkerbuijk et al., 2012). Thus, we suspect that the inhibition of BUB1B increased the phosphorylation and expression of kinase substrates either directly or indirectly through PLK1, or possibly via another polo-like kinase family member. Although we did not evaluate its expression in this study, maternally inherited genotypic variants spanning *PLK4* have also been reported to play a role in tripolar divisions and aneuploidy

Development (2022) 149, dev198341. doi:10.1242/dev.198341

in human embryos (McCoy et al., 2015a, 2018). Whether PLK4 similarly regulates BUB1B function is currently unknown, but BUB1B likely cooperates with a large regulatory network of kinases and their substrates to reinforce MCC function and ensure chromosome fidelity until ZGA. Collectively, our findings confirm that the MCC does indeed maintain proper chromosome segregation in the initial cleavage divisions of mammalian preimplantation development and show that deficiency in BUB1B and/or other maternally derived factors likely contributes to the karyotypic complexity observed in early embryos.

MATERIALS AND METHODS

Experimental design

Using a combination of live-cell imaging, scDNA-seq for CNV analysis and genetic manipulation of embryos, we developed an experimental approach to assess mitotic divisions and chromosome segregation throughout bovine preimplantation development (Fig. 1A). First, we fertilized mature oocytes, cultured resultant zygotes under a time-lapse imaging microscope to monitor embryo developmental dynamics, and evaluated DNA integrity and nuclear structure by immunofluorescence up to blastocyst stage (n=53). We confirmed our findings by live-cell confocal microscopy of zygotes microinjected with fluorescently labeled modified mRNAs and visualization of the initial mitotic divisions in real time (n=90). Cleavage-stage embryos between 2 and 12 cells were then disassembled into single blastomeres for comprehensive assessment of meiotic and/or mitotic errors (n=38). Finally, the role of the MCC in aneuploidy generation was determined by microinjecting zygotes with BUB1B MAOs (n=84) or a Std Control MAO (n=81) for comparison with non-injected embryos (n=180) and with embryos co-injected with BUB1B MAO and BUB1B modified mRNA (n=85) using time-lapse monitoring, immunostaining, CNV analysis and/or microfluidic quantitative RT-PCR.

Reagents and media

All chemicals were obtained from Sigma-Aldrich or ThermoFisher Scientific unless otherwise stated. Tyrode's albumin lactate pyruvate (TALP) medium with Hepes (TALP-Hepes) was used as washing media and contained 114 mM NaCl, 3.2 mM KCl, 25 mM $NaHCO_3$, 0.34 mM NaH_2PO_4-H_2O, 10 mM $C_3H_5NaO_3$, 2 mM $CaCl_2$-H_2O, 0.5 mM $MgCl_2$-$6H_2O$, 10.9 mM Hepes, 0.25 mM sodium pyruvate, 1 µl/ml Phenol Red, 3 mg/ml FAF-BSA and 100 µM gentamicin sulfate. For fertilization, TALP-IVF was used (114 mM NaCl, 3.2 mM KCl, 25 mM $NAHCO_3$, 0.34 mM NaH_2PO_4-H_2O, 10 mM $C_3H_5NaO_3$, 2 mM $CaCl_2$-H_2O, 0.5 mM $MgCl_2$-$6H_2O$, 1 µl/ml Phenol Red, 0.25 mM sodium pyruvate, 100 units/ml penicillin, 100 µg/ml streptomycin, 1 µM epinephrine, 0.02 mM penicillamine, 10 µM hypotaurine, 6 mg/ml FAF-BSA and 10 mg/ml heparin).

IVF and embryo culture

Cumulus-oocyte complexes (COCs) were retrieved by follicular aspiration of ovaries collected at a commercial abattoir (DeSoto Biosciences). Those COCs with at least three layers of compact cumulus cells and homogeneous cytoplasm were placed in groups of 50 in 2 ml sterile glass vials containing 1 ml of oocyte maturation medium, covered with mineral oil and equilibrated in 5% CO_2. Tubes with COCs were shipped overnight in a portable incubator (Minitube) at 38.5°C. Following 24 h of maturation, COCs were washed three times in TALP-Hepes followed by a final wash in fertilization media, before placement in a four-well dish (Nunc; ThermoFisher Scientific) containing 0.5 ml of fertilization media. Semen from either Racer (014HO07296, Accelerated Genetics) or Colt P-red (7HO10904, Select Sires) was obtained for IVF. Sperm were purified from frozen-thawed straws using a gradient [50% (v/v) and 90% (v/v)] of Isolate (Irvine Scientific), washed twice in fertilization media by centrifugation at 100 ***g***, and diluted to a final concentration of 1 million/ml in the fertilization dish. Fertilization was allowed to commence for 17-19 h at 38.5°C in a humidified atmosphere of 5% CO_2. Zygotes were denuded from the surrounding cumulus cells by vortexing for 4 min in 200 µl of TALP-Hepes with 0.5% (w/v) hyaluronidase (Sigma-Aldrich) and washed in fresh TALP-Hepes.

Time-lapse imaging

Denuded zygotes were transferred to custom Eeva 12-well polystyrene dishes (Progyny, formerly Auxogyn) containing 100 µl drops of BO-IVC culture media (IVF Bioscience) under mineral oil (CooperSurgical) and cultured at 38.5°C in a humidified atmosphere of 5% CO_2, 5% O_2 and 90% N_2. Embryos were monitored with an Eeva darkfield 2.2.1 or bimodal (darkfield/brightfield) 2.3.5 time-lapse microscope system (Progyny) housed in a small tri-gas incubator (Panasonic Healthcare) as previously described (Vera-Rodriguez et al., 2015). Images were taken every 5 min with a 0.6 s exposure time. Each image was time stamped with a frame number and all images compiled into an AVI movie using FIJI software version 2.0.0 (Schindelin et al., 2012) for assessment of mitotic divisions by two independent reviewers.

Immunofluorescent labeling

Embryos were washed in PBS with 0.1% BSA and 0.1% Tween-20 (PBST; Calbiochem), and fixed with 4% paraformaldehyde (Alfa Aesar) in PBST for 20 min at room temperature. Once fixed, the embryos were washed with gentle shaking three times for a total of 15 min in PBS-T to remove residual fixative. Embryos were permeabilized in 1% Triton-X (Calbiochem) for 1 h at room temperature and washed in PBST as described above. To block non-specific antibody binding, embryos were transferred to a 7% donkey serum (Jackson ImmunoResearch Laboratories)/PBS-T solution for either 1 h at room temperature or overnight at 4°C. An antibody against LMNB1 (ab16048, Abcam) was diluted 1:1000, while the CDX2 mouse monoclonal antibody (clone CDX2-88, Abcam) and ANXA2 rabbit monoclonal antibody (8235, Cell Signaling Technology) were diluted 1:100 in PBS-T with 1% donkey serum, and embryos stained for 1 h at room temperature or overnight at 4°C. The specificity of the ANXA2 antibody was tested by co-staining a highly-pure day 28 immortalized rhesus placental (iRP) first trimester trophoblast cell line, iRP-D28A (Rosenkrantz et al., 2021), using a mouse monoclonal antibody (clone OV-TL 12/30, Agilent Dako) to the pan-trophoblast marker cytokeratin 7 (KRT7). Primary immunosignals were detected using 488-conjugated donkey anti-rabbit (for LMNB1) or 647-conjugated donkey anti-mouse (for CDX2) Alexa Fluor secondary antibodies (Thermo Fisher Scientific) at a 1:250 dilution with 1% donkey serum in PBS-T at room temperature for 1 h in the dark. Embryos were washed in PBS-T and the DNA stained with either 1 µg/ml DAPI or Hoechst 34580 (Thermo Fisher) for 15 min. Embryos were mounted on slides using Prolong Diamond mounting medium (Invitrogen). Immunofluorescence was initially visualized on a Nikon Eclipse Ti-U fluorescent microscope system and images captured using a Nikon DS-Ri2 color camera and confirmed with a Leica SP5 AOBS spectral confocal system. *Z*-stacks, 1-5 µm apart, were imaged one fluorophore at a time to avoid spectral overlap between channels. Stacked images and individual channels for each color were combined into composite images using FIJI software version 2.0.0.

Modified mRNA construction

Plasmids containing the coding sequence (CDS) for mCitrine-Lifeact (Addgene 54733), which labels filamentous actin (F-actin), mCherry-Histone H2B-C-10 (Addgene 55057) and mCherry-LAMINB1-10 (Addgene 55069) were generated in Dr Michael Davidson's laboratory (National High Magnetic Field Laboratory and Department of Biological Science, Florida State University, USA). Custom primers containing a 5′-T7 promoter sequence were used to amplify each fluorescent tag-mRNA fusion construct as follows: T7_mCitrine_F, CTAGCTTAATACGACTCACTATAGGGCGGTCGCCACCATGGTGA; LifeAct_R, TTACTTGTACAGCTCGTCCATGCCGAGAGTGATCCCGGC; T7_mCherry_F, AATTAATACGACTCACTATAGGGAGAGCCACCATGGTGAGCAA; H2B_R, GCGGCCGCTTTACTTGT; and LAMINB1_R, TCCGGTGGATCCCTACATAA.

PCR amplification was performed with high-fidelity Platinum Taq polymerase (Thermo Fisher) under the following conditions: 94°C for 2 min, followed by 35 cycles of 94°C for 30 s, 70°C for 30 s and 72°C for

Development (2022) 149, dev198341. doi:10.1242/dev.198341

3 min. PCR products were purified with the QIAquick PCR Purification kit (Qiagen), then *in vitro* transcribed using the mMessage Machine T7 Transcription Kit (Invitrogen). Following the synthesis of capped mRNA, the MEGAclear transcription clean up kit (Invitrogen) was used to purify and concentrate the final modified mRNA product.

Live-cell imaging

Bovine zygotes were microinjected with mCitrine-Lifeact and either mCherry-H2B or mCherry-LAMINB1 mRNAs at a concentration of 20 ng/µl each in the presence of Alexa Fluor 488 labeled Dextran (Invitrogen) using a CellTram vario, electronic microinjector and Transferman NK 2 Micromanipulators (Eppendorf). Zygotes that exhibited mCherry fluorescent signal within 4-6 h of microinjection were selected for overnight imaging. Imaging dishes were prepared by placing 20 µl drops of BO-IVC media on glass-bottomed dishes (Matek) and covering with mineral oil. A Zeiss LSM 880 laser-scanning confocal microscope with 10× objective and Fast Airy capabilities was used to capture fluorescent images of embryos for 18-20 h, which encompassed the first three mitotic divisions. *Z*-stack images were taken every 1.5 µm for a total of 60 slices covering a 90 µm range at 10 min intervals. Each fluorophore was acquired independently to prevent crosstalk and maximize scanning speed. Individual images underwent Airyscan processing using Zeiss software and were compiled into videos with individual embryo labels using FIJI. Assessment of cytoplasmic and nuclear structure in embryos during mitotic divisions was completed by two independent reviewers.

Embryo disassembly

Embryos were disassembled under a stereomicroscope equipped with a heated stage and digital camera (Leica Microsystems) for documentation. The zona pellucida (ZP) was removed from each embryo by a 30 s exposure to warm Acidified Tyrode's Solution (EMD Millipore), followed by 30-60 s in 0.1% (w/v) pronase (Sigma-Aldrich). Once the ZP had been removed, embryos were washed in TALP-Hepes and gently manipulated using a STRIPPER pipettor (Origio), with or without brief exposure to warm 0.05% trypsin-EDTA (Thermo Fisher) as necessary, until all blastomeres were separated. Following disassembly, each blastomere and was washed three times with Ca^{2+} and Mg^{2+}-free PBS (Fisher Scientific), collected into individual PCR tubes in 2 µl of PBS and snap frozen on dry ice. Downstream analysis was completed only for embryos where the disassembly process was successful for all blastomeres.

DNA library preparation

Single bovine blastomeres and unaffected male (GM06034; 60XY) and female (GM06035; 60XX) skin fibroblasts from the Coriell Institute (Camden, NJ, USA) underwent DNA extraction and WGA using the PicoPLEX single-cell WGA Kit (Rubicon Genomics) according to the manufacturer's instructions with slight modifications. Cells were lysed at 75°C for 10 min followed by pre-amplification at 95°C for 2 min and 12 cycles of gradient PCR with PicoPLEX pre-amp enzyme and primer mix. Pre-amplified DNA was further amplified with PicoPLEX amplification enzyme and 48 uniquely indexed Illumina sequencing adapters provided by the kit or custom adapters with indices designed as previously described (Vitak et al., 2017; Daughtry et al., 2019). Adapter PCR amplification consisted of a 95°C hot start for 4 min, four cycles of 95°C for 20 s, 63°C for 25 s and 72°C for 40 s, and seven cycles of 95°C for 20 s and 72°C for 55 s. Libraries were quantified with a Qubit High Sensitivity (HS) DNA assay (Life Technologies). Amplified DNA from each blastomere and fibroblast (50 ng) was pooled and purified with AMPure XP beads (Beckman Coulter). Final library quality assessment was performed on a 2200 TapeStation (Agilent).

Multiplex scDNA-seq

Pooled libraries were sequenced on an Illumina NextSeq 500 using a 75-cycle kit with a modified single-end workflow that incorporated 14 dark cycles at the start of the first read prior to the imaged cycles. This step excluded the quasi-random priming sequences that are G-rich and lack a fluorophore for the two-color chemistry used by the NextSeq platform during cluster assignment. A total of 3.5×10^6 reads/sample were generated. All raw sample reads were demultiplexed and sequencing quality assessed with FastQC (Krueger et al., 2011). Illumina adapters were removed from raw reads with the sequence grooming tool, Cutadapt (Chen et al., 2014), which trimmed 15 bases on the 5′ end and five bases from the 3′ end, resulting in reads of 120 bp on average. Trimmed reads were aligned to the most recent bovine reference genome, BosTau8 (Zimin et al., 2009), using the BWA-MEM option of the Burrows-Wheeler Alignment Tool with default alignment parameters (Salavert Torres et al., 2012). Resulting bam files were filtered to remove alignments with quality scores below 30 (Q<30) as well as alignment duplicates that were likely the result of PCR artifacts with the Samtools suite (Ramirez-Gonzalez et al., 2012). The average number of filtered and uniquely mapped sequencing reads in individual libraries was between 1.9 and 2.2 million.

CNV analysis

CNV was determined by comparing a sample (blastomeres) to a known euploid control (fibroblasts) using the integration of two previously developed bioinformatics pipelines (Vitak et al., 2017): variable non-overlapping window circular binary segmentation (VNOWC) and the circular binary segmentation/hidden Markov model (CBS/HMM) intersect termed CHI, which we validated using cells with known aneuploidies (Daughtry et al., 2019). All CNV calls from the two pipelines generated profiles of variable-sized windows that were intersected on a window-by-window basis. Because other low-input sequencing studies have shown that CNV can be reliably assessed at a 15 Mb resolution with 0.5-1× genome coverage (Lee et al., 2013; Zhou et al., 2018), we classified breaks of 15 Mb in length or larger that did not affect the whole chromosome as segmental. Only whole and segmental CNV calls in agreement between the VNOWC and CHI methods at window sizes containing 4000 reads were considered. Chaotic aneuploidy was classified by the loss or gain of greater than four whole and/or broken chromosomes, as previously described (Daughtry et al., 2019). Additional classification of each aneuploidy as meiotic or mitotic in origin was accomplished by determining whether a loss or gain of the same chromosome was detected in all blastomeres (meiotic) or whether reciprocal chromosome losses and gains were observed between blastomeres (mitotic). Non-reciprocal chromosome losses and gains were also classified as mitotic errors and embryos containing blastomeres with both reciprocal and non-reciprocal mitotic errors of the same chromosome were only counted once.

MAO design and labeling

Two non-overlapping MAOs were designed and synthesized by Gene Tools to specifically target bovine BUB1B (Ensembl transcript ID: ENSBTAT00000009521.5). BUB1B MAO 1 (TTTCCTTCTGCATCGCC-GCCATC) specifically targeted the ATG start codon of the BUB1B mRNA-coding sequence, while BUB1B MAO 2 (CGATCTGAGGCTCTGAA-GAAAGGCC) targeted upstream of MAO 1 in the 5′ UTR of bovine *BUB1B*. A Std Control MO (CCTCTTACCTCAGTTACAATTTATA) that targets a splice site mutant of the human hemoglobin β-chain (HBB) gene (GenBank accession number AY605051) that is not present in the *Bos taurus* genome served as a control. Both BUB1B and Std Control MAO were synthesized with a 3′-carboxyfluorescein tag to aid in visualization during cell transfection and embryo manipulation.

Assessment of BUB1B knockdown in MDBK cells by immunofluorescence

Before use in embryos, the BUB1B MAOs were first tested using the MDBK epithelial cell line (Madin and Darby, 1958). MDBK cells were plated on poly-L-lysine treated coverslips and grown to 70% confluency prior to MAO treatment. The cells were incubated with 6 µl/ml Endo-Porter delivery reagent containing DMSO (Gene Tools) and 2, 4 or 8 µM of either BUB1B MAO 1 or Std control MAO and cultured in Eagle's Minimum Essential Medium modified to contain Earle's Balanced Salt Solution, non-essential amino acids, 2 mM L-glutamine, 1 mM sodium pyruvate, 1500 mg/l sodium bicarbonate, 10% (v/v) FBS and antibiotics (50 U penicillin and 50 µg streptomycin) in 5% CO_2 at 37°C. After 36 h, cells were synchronized at metaphase in the presence of 0.03 µg of colcemid (Sigma-Aldrich) for 12 h,

Development (2022) 149, dev198341. doi:10.1242/dev.198341

and collected for staining at 48 h post MAO treatment. Cells were washed in PBS, followed by a single 20 min fixation using 4% paraformaldehyde (Alfa Aesar) and a permeabilization step with 1% Triton-X (Calbiochem) in PBS. Additional PBS washes were completed prior to blocking with 7% donkey serum (Jackson ImmunoResearch Laboratories) in PBS for either 1 h at room temperature or overnight at 4°C. A primary antibody against BUB1B (ab28193, Abcam) was diluted 1:1000 in PBS with 1% donkey serum, and cells were incubated overnight at 4°C. BUB1B antibody binding was detected using a 568-conjugated donkey anti-rabbit Alexa Fluor secondary antibody (Thermo Fisher) at a 1:250 dilution with 1% donkey serum in PBS at room temperature for 1 h in the dark. Cells were washed in PBS and the DNA stained with 1 µg/ml DAPI for 15 min. The coverslips with adherent cells were then mounted on slides using Prolong Diamond mounting medium (Invitrogen). Immunofluorescence was visualized on a Nikon Eclipse Ti-U fluorescent microscope system and representative fluorescent images captured with a Nikon DS-Ri2 color camera. Using FIJI, background fluorescence was subtracted from the red (BUB1B) channel, followed by individual channels of each color for combination into a composite image. BUB1B immunostaining was visually assessed at each MAO concentration for 100 metaphase cells per treatment group.

Western blot analysis of BUB1B expression in MDBK cells

To confirm sufficient BUB1B knockdown, MDBK cells were treated with or without colcemid, as described above, before mitotic shake-off (Ligasová and Koberna, 2021) and lysed in RIPA Buffer (Sigma-Aldrich) with a protease inhibitor cocktail (Thermo Fisher). Protein concentrations were calculated by BCA assay (Thermo Fisher) and a total of 20 µg of total cellular protein was loaded per lane. Proteins were separated by SDS-PAGE using 12% polyacrylamide gels (Sigma-Aldrich) and transferred to Immun-Blot PVDF membranes (Bio-Rad). Nonspecific binding was inhibited by blocking the membranes in 5% BSA (Sigma-Aldrich) before immunoblotting. Membranes were incubated overnight at 4°C with the BUB1B primary antibody described above at a 1:1000 dilution, followed by a 1:5000 dilution of a 488-conjugated donkey anti-rabbit Alexa Fluor secondary antibody (Thermo Fisher) for 1 h at room temperature. Incubation with an α-tubulin primary antibody (clone TU-01, Thermo Fisher) diluted 1:1000, followed by a 1:3000 dilution of a 647-conjugated donkey anti-mouse Alexa Fluor secondary antibody (Thermo Fisher) served as a loading control. After each step, the membranes were washed three times with TBST for 10 min. Finally, the blots were visualized using a FluoroChem M fluorescence and chemiluminescence imaging system (Protein Simple), and the images processed in FIJI.

BUB1B knockdown and validation in embryos

Zygotes underwent cytoplasmic injection with 3′-carboxyfluorescein-labeled MAO at 20 h post fertilization as described above. A concentration of 0.3 mM MAO was used based on previous findings that Std Control MAO at this concentration was the maximum that allowed normal blastocyst formation rates. Following microinjection, embryos were cultured up to the blastocyst stage as described above with or without imaging on the Eeva darkfield 2.2.1 microscope system. Upon developmental arrest, embryos were collected for immunostaining, gene expression analysis or for disassembly into single cells (as described above) for downstream analysis. To further validate MAO specificity, bovine embryos were co-injected with BUB1B-modified mRNA at a concentration of ∼3 nl (75 pg) of mRNA per embryo in addition to BUB1B MAO 1. The BUB1B-coding sequence (CDS) was amplified from the plasmid, pcDNA5-EGFP-AID-BubR1 (Addgene 47330), followed by mutation of the MAO binding site using the Q5 site-directed mutagenesis kit (NEB) according to the manufacturer's instructions. Briefly, custom primers (forward, 5′-aa-aaaagagggaGGTGCTCTGAGTGAAGCC-3′; and reverse, 5′-aactgcagcca-tATGGGATCCAGCTCTGCT-3′) were designed to mutate the region of the BUB1B CDS targeted by the MAO without affecting the amino acid sequence. The uppercase letters indicate the targeting sequence; the lowercase letters are the 'backbone sequence' containing 5′ and 3′ UTRs. Exponential amplification of the template plasmid using high-fidelity DNA polymerase was followed by a single step phosphorylation, ligation and DpnI restriction enzyme digestion. NEB 5-α competent cells were transformed with the mutated plasmid, followed by DNA miniprep isolation using QIAprep spin columns (Qiagen). Mutated plasmids were identified by Sanger sequencing performed by the ONPRC Molecular and Cellular Biology Core using a custom designed primer (TTGGTGAATAGCTGG-GACTATG). Following identification and isolation, the mutated plasmid served as a template to synthesize a PCR product containing a T7 promoter using Platinum Taq (Invitrogen). Custom primers (forward, CTAGCTTAA TACGACTCACTATAGGGAGCGCCACCATGGCTGCAGTTAAAAAA GAG; reverse, CAATCTGTGAGACTTGATTGCCTAGCTCACTGAA AGAGCAAAGCCCCAG) were designed for use with the T7 mMessage mMachine Ultra Kit as described above.

Quantitative RT-PCR analysis

Gene expression was analyzed in non-injected, Std control MAO- or BUB1B MAO-injected embryos using the BioMark Dynamic Array microfluidic system (Fluidigm). All embryos were collected within 36 h of fertilization as described above. Individual embryos were pre-amplified according to the manufacturer's 'two-step single cell gene expression' protocol (Fluidigm) using a SuperScript VILO cDNA synthesis kit (Invitrogen), TaqMan PreAmp Master Mix (Applied Biosystems) and gene-specific primers designed to span exons using Primer-BLAST (NCBI). Bovine fibroblasts and no reverse transcription template samples were used as controls. Pre-amplified cDNA was loaded into the sample inlets of a 96×96 dynamic array (DA; Fluidigm) and assayed in triplicate. Genes that exhibited no or very little expression, despite the design and testing of multiple primer sets, were removed from further analysis. A total of 10 reference genes were assayed for use as relative expression controls. Cycle threshold (Ct) values were normalized to the two most stable housekeeping genes (*RPL15* and *GUSB*) using qBase^{+} 3.2 software (Biogazelle). The mean was determined from the calculated normalized relative quantity (CNRQ) values across triplicates±s.e.m. and plotted using Morpheus (https://software.broadinstitute.org/morpheus/).

Statistical analysis

To determine statistical differences between MAO concentrations in MDBK cells, log-binomial modeling using the Generalized Estimating Equations approach was performed and Tukey's test adjusted *P*-values reported to adjust for multiple comparisons. For the RT-qPCR results, the Mann–Whitney *U*-test was used for nonparametric multiple comparisons with Bonferroni correction. An unadjusted $P \leq 0.05$ was considered statistically significant.

Acknowledgements

We gratefully acknowledge Dr Tom Spencer at the University of Missouri-Columbia for the Madin-Darby Bovine Kidney (MDBK) epithelial cells. Drs Crystal Chaw and Stefanie Kaech Petrie in the OHSU Advanced Light Microscopy (ALM) Core were instrumental in developing our imaging protocol, and we very much appreciate all their help and support. We also thank Drs Andrew Adey and Andrew Fields for their assistance and use of the NextSeq500 sequencer. We acknowledge the Oregon National Primate Research Center (ONPRC) Integrated Pathology Core for confocal microscopy (supported by S10RR024585) that operates under the auspices of the ONPRC NIH/OD core grant (P51OD011092).

Competing interests

The authors declare no competing or financial interests.

Author contributions

Conceptualization: K.E.B., S.L.C.; Methodology: K.E.B., B.L.D., S.L.C.; Software: K.E.B., B.D., M.Y.Y.; Validation: K.E.B., S.S., S.L.C.; Formal analysis: K.E.B., S.L.C.; Investigation: K.E.B., B.L.D.; Data curation: S.S.F., S.L.C.; Writing - original draft: K.E.B., S.L.C.; Writing - review & editing: K.E.B., B.L.D., B.D., M.Y.Y., S.S.F., S.S., L.C., S.L.C.; Visualization: K.E.B., B.D., M.Y.Y.; Supervision: S.S.F., L.C., S.L.C.; Project administration: S.L.C.; Funding acquisition: K.E.B., L.C., S.L.C.

Funding

K.E.B. was supported by the National Institutes of Health/Eunice Kennedy Shriver National Institute of Child Health and Human Development Postdoctoral Individual National Research Service Award (5F32HD095550-01). B.L.D. was supported by a P.E.O. Scholar Award, a N. L. Tartar Research Fellowship and a T32 Reproductive Biology National Institutes of Health Training Grant (T32 HD007133). This work was

supported by Oregon Health and Science University/Oregon National Primate Research Center start-up funds (to S.L.C.) and by the National Institutes of Health/Eunice Kennedy Shriver National Institute of Child Health and Human Development (R01HD086073-A1). Open Access funding provided by Oregon Health and Science University. Deposited in PMC for immediate release.

Data availability

All sequencing data have been deposited in SRA under accession number PRJNA577965.

References

Alper, M. M., Brinsden, P., Fischer, R. and Wikland, M. (2001). To blastocyst or not to blastocyst? That is the question. *Hum. Reprod.* **16**, 617-619. doi:10.1093/humrep/16.4.617

Baker, D. J., Jeganathan, K. B., Cameron, J. D., Thompson, M., Juneja, S., Kopecka, A., Kumar, R., Jenkins, R. B., de Groen, P. C., Roche, P. et al. (2004). BubR1 insufficiency causes early onset of aging-associated phenotypes and infertility in mice. *Nat. Genet.* **36**, 744-749. doi:10.1038/ng1382

Baker, D. J., Dawlaty, M. M., Wijshake, T., Jeganathan, K. B., Malureanu, L., van Ree, J. H., Crespo-Diaz, R., Reyes, S., Seaburg, L., Shapiro, V. et al. (2013). Increased expression of BubR1 protects against aneuploidy and cancer and extends healthy lifespan. *Nat. Cell Biol.* **15**, 96-102. doi:10.1038/ncb2643

Baltaci, V., Satiroglu, H., Kabukçu, C., Ünsal, E., Aydinuraz, B., Üner, O., Aktas, Y., Çetinkaya, E., Turhan, F. and Aktan, A. (2006). Relationship between embryo quality and aneuploidies. *Reprod. Biomed. Online* **12**, 77-82. doi:10.1016/S1472-6483(10)60984-4

Bibi, N., Parveen, Z. and Rashid, S. (2013). Identification of potential Plk1 targets in a cell-cycle specific proteome through structural dynamics of kinase and Polo box-mediated interactions. *PLoS ONE* **8**, e70843. doi:10.1371/journal.pone.0070843

Bolton, H., Graham, S. JL., Van der Aa, N., Kumar, P., Theunis, K., Fernandez Gallardo, E., Voet, T. and Zernicka-Goetz, M. (2016). Mouse model of chromosome mosaicism reveals lineage-specific depletion of aneuploid cells and normal developmental potential. *Nat. Commun.* **7**, 11165. doi:10.1038/ncomms11165

Braude, P., Bolton, V. and Moore, S. (1988). Human gene expression first occurs between the four- and eight-cell stages of preimplantation development. *Nature* **332**, 459-461. doi:10.1038/332459a0

Cavazza, T., Takeda, Y., Politi, A. Z., Aushev, M., Aldag, P., Baker, C., Choudhary, M., Bucevičius, J., Lukinavičius, G., Elder, K. et al. (2021). Parental genome unification is highly error-prone in mammalian embryos. *Cell* **184**, 2860-2877.e22. doi:10.1016/j.cell.2021.04.013

Chavez, S. L., Loewke, K. E., Han, J., Moussavi, F., Colls, P., Munne, S., Behr, B. and Reijo Pera, R. A. (2012). Dynamic blastomere behaviour reflects human embryo ploidy by the four-cell stage. *Nat. Commun.* **3**, 1251. doi:10.1038/ncomms2249

Chavez, S. L., McElroy, S. L., Bossert, N. L., De Jonge, C. J., Rodriguez, M. V., Leong, D. E., Behr, B., Westphal, L. M. and Reijo Pera, R. A. (2014). Comparison of epigenetic mediator expression and function in mouse and human embryonic blastomeres. *Hum. Mol. Genet.* **23**, 4970-4984. doi:10.1093/hmg/ddu212

Chen, C., Khaleel, S. S., Huang, H. and Wu, C. H. (2014). Software for pre-processing Illumina next-generation sequencing short read sequences. *Source Code Biol. Med.* **9**, 8. doi:10.1186/1751-0473-9-8

Crasta, K., Ganem, N. J., Dagher, R., Lantermann, A. B., Ivanova, E. V., Pan, Y., Nezi, L., Protopopov, A., Chowdhury, D. and Pellman, D. (2012). DNA breaks and chromosome pulverization from errors in mitosis. *Nature* **482**, 53-58. doi:10.1038/nature10802

Daughtry, B. L., Rosenkrantz, J. L., Lazar, N. H., Fei, S. S., Redmayne, N., Torkenczy, K. A., Adey, A., Yan, M., Gao, L., Park, B. et al. (2019). Single-cell sequencing of primate preimplantation embryos reveals chromosome elimination via cellular fragmentation and blastomere exclusion. *Genome Res.* **29**, 367-382. doi:10.1101/gr.239830.118

Destouni, A., Zamani Esteki, M., Catteeuw, M., Tšuiko, O., Dimitriadou, E., Smits, K., Kurg, A., Salumets, A., Van Soom, A., Voet, T. et al. (2016). Zygotes segregate entire parental genomes in distinct blastomere lineages causing cleavage-stage chimerism and mixoploidy. *Genome Res.* **26**, 567-578. doi:10.1101/gr.200527.115

Elowe, S., Hümmer, S., Uldschmid, A., Li, X. and Nigg, E. A. (2007). Tension-sensitive Plk1 phosphorylation on BubR1 regulates the stability of kinetochore-microtubule interactions. *Genes Dev.* **21**, 2205-2219. doi:10.1101/gad.436007

Elowe, S., Dulla, K., Uldschmid, A., Li, X., Dou, Z. and Nigg, E. A. (2010). Uncoupling of the spindle-checkpoint and chromosome-congression functions of BubR1. *J. Cell Sci.* **123**, 84-94. doi:10.1242/jcs.056507

Fang, G. (2002). Checkpoint protein BubR1 acts synergistically with Mad2 to inhibit anaphase-promoting complex. *Mol. Biol. Cell* **13**, 755-766. doi:10.1091/mbc.01-09-0437

Fiorentino, F., Bono, S., Biricik, A., Nuccitelli, A., Cotroneo, E., Cottone, G., Kokocinski, F., Michel, C.-E., Minasi, M. G. and Greco, E. (2014). Application of next-generation sequencing technology for comprehensive aneuploidy screening of blastocysts in clinical preimplantation genetic screening cycles. *Hum. Reprod.* **29**, 2802-2813. doi:10.1093/humrep/deu277

Fragouli, E., Alfarawati, S., Spath, K. and Wells, D. (2014). Morphological and cytogenetic assessment of cleavage and blastocyst stage embryos. *Mol. Hum. Reprod.* **20**, 117-126. doi:10.1093/molehr/gat073

Fragouli, E., Alfarawati, S., Spath, K., Babariya, D., Tarozzi, N., Borini, A. and Wells, D. (2017). Analysis of implantation and ongoing pregnancy rates following the transfer of mosaic diploid-aneuploid blastocysts. *Hum. Genet.* **136**, 805-819. doi:10.1007/s00439-017-1797-4

Ganem, N. J., Godinho, S. A. and Pellman, D. (2009). A mechanism linking extra centrosomes to chromosomal instability. *Nature* **460**, 278-282. doi:10.1038/nature08136

Garrido-Gómez, T., Dominguez, F., Quiñonero, A., Estella, C., Vilella, F., Pellicer, A. and Simon, C. (2012). Annexin A2 is critical for embryo adhesiveness to the human endometrium by RhoA activation through F-actin regulation. *FASEB J.* **26**, 3715-3727. doi:10.1096/fj.12-204008

Gasca, S., Pellestor, F., Assou, S., Loup, V., Anahory, T., Dechaud, H., De Vos, J. and Hamamah, S. (2007). Identifying new human oocyte marker genes: a microarray approach. *Reprod. Biomed. Online* **14**, 175-183. doi:10.1016/S1472-6483(10)60785-7

Gilbert, S. (2000). Early mammalian development. In *Developmental Biology* (6th edn), p. 709.

Gjorret, J. O., Knijn, H. M., Dieleman, S. J., Avery, B., Larsson, L. I. and Maddox-Hyttel, P. (2003). Chronology of apoptosis in bovine embryos produced in vivo and in vitro. *Biol. Reprod.* **69**, 1193-1200. doi:10.1095/biolreprod.102.013243

Gosden, R., Trasler, J., Lucifero, D. and Faddy, M. (2003). Rare congenital disorders, imprinted genes, and assisted reproductive technology. *Lancet* **361**, 1975-1977. doi:10.1016/S0140-6736(03)13592-1

Greco, E., Minasi, M. G. and Fiorentino, F. (2015). Healthy babies after intrauterine transfer of mosaic aneuploid blastocysts. *N. Engl. J. Med.* **373**, 2089-2090. doi:10.1056/NEJMc1500421

Griffiths, J. A., Scialdone, A. and Marioni, J. C. (2017). Mosaic autosomal aneuploidies are detectable from single-cell RNAseq data. *BMC Genomics* **18**, 904. doi:10.1186/s12864-017-4253-x

Hassold, T., Chen, N., Funkhouser, J., Jooss, T., Manuel, B., Matsuura, J., Matsuyama, A., Wilson, C., Yamane, J. A. and Jacobs, P. A. (1980). A cytogenetic study of 1000 spontaneous abortions. *Ann. Hum. Genet.* **44**, 151-178. doi:10.1111/j.1469-1809.1980.tb00955.x

Hattori, H., Hiura, H., Kitamura, A., Miyauchi, N., Kobayashi, N., Takahashi, S., Okae, H., Kyono, K., Kagami, M., Ogata, T. et al. (2019). Association of four imprinting disorders and ART. *Clin. Epigenet.* **11**, 21. doi:10.1186/s13148-019-0623-3

Held, L. I.Jr. (1982). Polyploidy and aneuploidy by colcemid in Drosophila melanogaster. *Mutat. Res.* **94**, 87-101. doi:10.1016/0027-5107(82)90171-3

Hornak, M., Kubicek, D., Broz, P., Hulinska, P., Hanzalova, K., Griffin, D., Machatkova, M. and Rubes, J. (2016). Aneuploidy detection and mtDNA quantification in bovine embryos with different cleavage onset using a next-generation sequencing-based protocol. *Cytogenet Genome Res.* **150**, 60-67. doi:10.1159/000452923

Kai, Y., Moriwaki, H., Yumoto, K., Iwata, K. and Mio, Y. (2018). Assessment of developmental potential of human single pronucleated zygotes derived from conventional in vitro fertilization. *J. Assist. Reprod. Genet.* **35**, 1377-1384. doi:10.1007/s10815-018-1241-2

Kettenbach, A. N., Schweppe, D. K., Faherty, B. K., Pechenick, D., Pletnev, A. A. and Gerber, S. A. (2011). Quantitative phosphoproteomics identifies substrates and functional modules of Aurora and Polo-like kinase activities in mitotic cells. *Sci. Signal.* **4**, rs5. doi:10.1126/scisignal.2001497

Kiessling, A. A., Bletsa, R., Desmarais, B., Mara, C., Kallianidis, K. and Loutradis, D. (2010). Genome-wide microarray evidence that 8-cell human blastomeres over-express cell cycle drivers and under-express checkpoints. *J. Assist. Reprod. Genet.* **27**, 265-276. doi:10.1007/s10815-010-9407-6

Krueger, F., Andrews, S. R. and Osborne, C. S. (2011). Large scale loss of data in low-diversity illumina sequencing libraries can be recovered by deferred cluster calling. *PLoS ONE* **6**, e16607. doi:10.1371/journal.pone.0016607

Lampson, M. A. and Kapoor, T. M. (2005). The human mitotic checkpoint protein BubR1 regulates chromosome-spindle attachments. *Nat. Cell Biol.* **7**, 93-98. doi:10.1038/ncb1208

Lee, J., Lee, U., Kim, B. and Yoon, J. (2013). A computational method for detecting copy number variations using scale-space filtering. *BMC Bioinformatics* **14**, 57. doi:10.1186/1471-2105-14-57

Li, D., Morley, G., Whitaker, M. and Huang, J.-Y. (2010). Recruitment of Cdc20 to the kinetochore requires BubR1 but not Mad2 in Drosophila melanogaster. *Mol. Cell. Biol.* **30**, 3384-3395. doi:10.1128/MCB.00258-10

Ligasová, A. and Koberna, K. (2021). Strengths and weaknesses of cell synchronization protocols based on inhibition of DNA synthesis. *Int. J. Mol. Sci.* **22**, 10759. doi:10.3390/ijms221910759
Madin, S. H. and Darby, N. B.Jr. (1958). Established kidney cell lines of normal adult bovine and ovine origin. *Proc. Soc. Exp. Biol. Med.* **98**, 574-576. doi:10.3181/00379727-98-24111
Magli, M. C., Jones, G. M., Gras, L., Gianaroli, L., Korman, I. and Trounson, A. O. (2000). Chromosome mosaicism in day 3 aneuploid embryos that develop to morphologically normal blastocysts in vitro. *Hum. Reprod.* **15**, 1781-1786. doi:10.1093/humrep/15.8.1781
Mantikou, E., Wong, K. M., Repping, S. and Mastenbroek, S. (2012). Molecular origin of mitotic aneuploidies in preimplantation embryos. *Biochim. Biophys. Acta* **1822**, 1921-1930. doi:10.1016/j.bbadis.2012.06.013
Mayer, W., Smith, A., Fundele, R. and Haaf, T. (2000). Spatial separation of parental genomes in preimplantation mouse embryos. *J. Cell Biol.* **148**, 629-634. doi:10.1083/jcb.148.4.629
McCoy, R. C., Demko, Z., Ryan, A., Banjevic, M., Hill, M., Sigurjonsson, S., Rabinowitz, M., Fraser, H. B. and Petrov, D. A. (2015a). Common variants spanning PLK4 are associated with mitotic-origin aneuploidy in human embryos. *Science* **348**, 235-238. doi:10.1126/science.aaa3337
McCoy, R. C., Demko, Z. P., Ryan, A., Banjevic, M., Hill, M., Sigurjonsson, S., Rabinowitz, M. and Petrov, D. A. (2015b). Evidence of selection against complex mitotic-origin aneuploidy during preimplantation development. *PLoS Genet.* **11**, e1005601. doi:10.1371/journal.pgen.1005601
McCoy, R. C., Newnham, L. J., Ottolini, C. S., Hoffmann, E. R., Chatzimeletiou, K., Cornejo, O. E., Zhan, Q., Zaninovic, N., Rosenwaks, Z., Petrov, D. A. et al. (2018). Tripolar chromosome segregation drives the association between maternal genotype at variants spanning PLK4 and aneuploidy in human preimplantation embryos. *Hum. Mol. Genet.* **27**, 2573-2585. doi:10.1093/hmg/ddy147
Middelkamp, S., van Tol, H. TA., Spierings, D. CJ., Boymans, S., Guryev, V., Roelen, B. AJ., Lansdorp, P. M., Cuppen, E. and Kuijk, E. W. (2020). Sperm DNA damage causes genomic instability in early embryonic development. *Sci. Adv.* **6**, eaaz7602. doi:10.1126/sciadv.aaz7602
Ottolini, C. S., Kitchen, J., Xanthopoulou, L., Gordon, T., Summers, M. C. and Handyside, A. H. (2017). Tripolar mitosis and partitioning of the genome arrests human preimplantation development in vitro. *Sci. Rep.* **7**, 9744. doi:10.1038/s41598-017-09693-1
Pérez-Mongiovi, D., Malmanche, N., Bousbaa, H. and Sunkel, C. (2005). Maternal expression of the checkpoint protein BubR1 is required for synchrony of syncytial nuclear divisions and polar body arrest in Drosophila melanogaster. *Development* **132**, 4509-4520. doi:10.1242/dev.02028
Petropoulos, S., Edsgard, D., Reinius, B., Deng, Q., Panula, S. P., Codeluppi, S., Reyes, A. P., Linnarsson, S., Sandberg, R. and Lanner, F. (2016). Single-cell RNA-seq reveals lineage and X chromosome dynamics in human preimplantation embryos. *Cell* **167**, 285. doi:10.1016/j.cell.2016.08.009
Plante, L., Shepherd, D. L., Allan King, W. and Plante, C. (1994). Cleavage and ^{3}H-uridine incorporation in bovine embryos of high in vitro developmental potential. *Mol. Reprod. Dev.* **39**, 375-383. doi:10.1002/mrd.1080390405
Popovic, M., Dheedene, A., Christodoulou, C., Taelman, J., Dhaenens, L., Van Nieuwerburgh, F., Deforce, D., Van den Abbeel, E., De Sutter, P., Menten, B. et al. (2018). Chromosomal mosaicism in human blastocysts: the ultimate challenge of preimplantation genetic testing? *Hum. Reprod.* **33**, 1342-1354. doi:10.1093/humrep/dey106
Ramirez-Gonzalez, R. H., Bonnal, R., Caccamo, M. and Maclean, D. (2012). Bio-samtools: Ruby bindings for SAMtools, a library for accessing BAM files containing high-throughput sequence alignments. *Source Code Biol. Med.* **7**, 6. doi:10.1186/1751-0473-7-6
Reichmann, J., Nijmeijer, B., Hossain, M. J., Eguren, M., Schneider, I., Politi, A. Z., Roberti, M. J., Hufnagel, L., Hiiragi, T. and Ellenberg, J. (2018). Dual-spindle formation in zygotes keeps parental genomes apart in early mammalian embryos. *Science* **361**, 189-193. doi:10.1126/science.aar7462
Rosenkrantz, J. L., Gaffney, J. E., Roberts, V. HJ., Carbone, L. and Chavez, S. L. (2021). Transcriptomic analysis of primate placentas and novel rhesus trophoblast cell lines informs investigations of human placentation. *BMC Biol.* **19**, 127. doi:10.1186/s12915-021-01056-7
Salavert Torres, J., Blanquer Espert, I., Dominguez, A. T., Hernandez Garcia, V., Medina Castello, I., Tarraga Gimenez, J. and Blazquez, J. D. (2012). Using GPUs for the exact alignment of short-read genetic sequences by means of the Burrows-Wheeler transform. *IEEE/ACM Trans. Comput. Biol. Bioinform.* **9**, 1245-1256. doi:10.1109/TCBB.2012.49
Santamaria, A., Wang, B., Elowe, S., Malik, R., Zhang, F., Bauer, M., Schmidt, A., Silljé, H. H. W., Körner, R. and Nigg, E. A. (2011). The Plk1-dependent phosphoproteome of the early mitotic spindle. *Mol. Cell. Proteomics* **10**, M110.004457. doi:10.1074/mcp.M110.004457
Schaeffer, A. J., Chung, J., Heretis, K., Wong, A., Ledbetter, D. H. and Lese Martin, C. (2004). Comparative genomic hybridization-array analysis enhances the detection of aneuploidies and submicroscopic imbalances in spontaneous miscarriages. *Am. J. Hum. Genet.* **74**, 1168-1174. doi:10.1086/421250
Schindelin, J., Arganda-Carreras, I., Frise, E., Kaynig, V., Longair, M., Pietzsch, T., Preibisch, S., Rueden, C., Saalfeld, S., Schmid, B. et al. (2012). Fiji: an open-source platform for biological-image analysis. *Nat. Methods* **9**, 676-682. doi:10.1038/nmeth.2019
Schneider, I. and Ellenberg, J. (2019). Mysteries in embryonic development: how can errors arise so frequently at the beginning of mammalian life? *PLoS Biol.* **17**, e3000173. doi:10.1371/journal.pbio.3000173
Schneider, I., de Ruijter-Villani, M., Hossain, M. J., Stout, T. AE. and Ellenberg, J. (2021). Dual spindles assemble in bovine zygotes despite the presence of paternal centrosomes. *J. Cell Biol.* **220**, e202010106. doi:10.1083/jcb.202010106
Schvartzman, J.-M., Sotillo, R. and Benezra, R. (2010). Mitotic chromosomal instability and cancer: mouse modelling of the human disease. *Nat. Rev. Cancer* **10**, 102-115. doi:10.1038/nrc2781
Simmons, A. J., Park, R., Sterling, N. A., Jang, M.-H., van Deursen, J. MA., Yen, T. J., Cho, S.-H. and Kim, S. (2019). Nearly complete deletion of BubR1 causes microcephaly through shortened mitosis and massive cell death. *Hum. Mol. Genet.* **28**, 1822-1836. doi:10.1093/hmg/ddz022
Singla, S., Iwamoto-Stohl, L. K., Zhu, M. and Zernicka-Goetz, M. (2020). Autophagy-mediated apoptosis eliminates aneuploid cells in a mouse model of chromosome mosaicism. *Nat. Commun.* **11**, 2958. doi:10.1038/s41467-020-16796-3
Soto, M., Raaijmakers, J. A. and Medema, R. H. (2019). Consequences of Genomic Diversification Induced by Segregation Errors. *Trends Genet.* **35**, 279-291. doi:10.1016/j.tig.2019.01.003
Starostik, M. R., Sosina, O. A. and McCoy, R. C. (2020). Single-cell analysis of human embryos reveals diverse patterns of aneuploidy and mosaicism. *Genome Res.* **30**, 814-825. doi:10.1101/gr.262774.120
Sugimura, S., Akai, T., Hashiyada, Y., Somfai, T., Inaba, Y., Hirayama, M., Yamanouchi, T., Matsuda, H., Kobayashi, S., Aikawa, Y. et al. (2012). Promising system for selecting healthy in vitro-fertilized embryos in cattle. *PLoS ONE* **7**, e36627. doi:10.1371/journal.pone.0036627
Suijkerbuijk, S. J. E., Vleugel, M., Teixeira, A. and Kops, G. J. (2012). Integration of kinase and phosphatase activities by BUBR1 ensures formation of stable kinetochore-microtubule attachments. *Dev. Cell* **23**, 745-755. doi:10.1016/j.devcel.2012.09.005
Treff, N. R., Krisher, R. L., Tao, X., Garnsey, H., Bohrer, C., Silva, E., Landis, J., Taylor, D., Scott, R. T., Woodruff, T. K. et al. (2016). Next generation sequencing-based comprehensive chromosome screening in mouse polar bodies, oocytes, and embryos. *Biol. Reprod.* **94**, 76. doi:10.1095/biolreprod.115.135483
Tšuiko, O., Catteeuw, M., Zamani Esteki, M., Destouni, A., Bogado Pascottini, O., Besenfelder, U., Havlicek, V., Smits, K., Kurg, A., Salumets, A. et al. (2017). Genome stability of bovine in vivo-conceived cleavage-stage embryos is higher compared to in vitro-produced embryos. *Hum. Reprod.* **32**, 2348-2357. doi:10.1093/humrep/dex286
Tšuiko, O., Jatsenko, T., Parameswaran Grace, L. K., Kurg, A., Vermeesch, J. R., Lanner, F., Altmäe, S. and Salumets, A. (2019). A speculative outlook on embryonic aneuploidy: can molecular pathways be involved? *Dev. Biol.* **447**, 3-13. doi:10.1016/j.ydbio.2018.01.014
Tutt, D. A. R., Silvestri, G., Serrano-Albal, M., Simmons, R. J., Kwong, W. Y., Guven-Ates, G., Canedo-Ribeiro, C., Labrecque, R., Blondin, P., Handyside, A. H. et al. (2021). Analysis of bovine blastocysts indicates ovarian stimulation does not induce chromosome errors, nor discordance between inner-cell mass and trophectoderm lineages. *Theriogenology* **161**, 108-119. doi:10.1016/j.theriogenology.2020.11.021
Vanneste, E., Voet, T., Le Caignec, C., Ampe, M., Konings, P., Melotte, C., Debrock, S., Amyere, M., Vikkula, M., Schuit, F. et al. (2009). Chromosome instability is common in human cleavage-stage embryos. *Nat. Med.* **15**, 577-583. doi:10.1038/nm.1924
Vazquez-Diez, C., Paim, L. M. G. and FitzHarris, G. (2019). Cell-size-independent spindle checkpoint failure underlies chromosome segregation error in mouse embryos. *Curr. Biol.* **29**, 865-873.e63. doi:10.1016/j.cub.2018.12.042
Vera-Rodriguez, M., Chavez, S. L., Rubio, C., Reijo Pera, R. A. R. and Simon, C. (2015). Prediction model for aneuploidy in early human embryo development revealed by single-cell analysis. *Nat. Commun.* **6**, 7601. doi:10.1038/ncomms8601
Vitak, S. A., Torkenczy, K. A., Rosenkrantz, J. L., Fields, A. J., Christiansen, L., Wong, M. H., Carbone, L., Steemers, F. J. and Adey, A. (2017). Sequencing thousands of single-cell genomes with combinatorial indexing. *Nat. Methods* **14**, 302-308. doi:10.1038/nmeth.4154
Wang, B. and Shao, Y. (2020). Annexin A2 acts as an adherent molecule under the regulation of steroids during embryo implantation. *Mol. Hum. Reprod.* **26**, 825-836. doi:10.1093/molehr/gaaa065
Webster, A. and Schuh, M. (2017). Mechanisms of Aneuploidy in Human Eggs. *Trends Cell Biol.* **27**, 55-68. doi:10.1016/j.tcb.2016.09.002
Wei, Y., Multi, S., Yang, C.-R., Ma, J., Zhang, Q.-H., Wang, Z.-B., Li, M., Wei, L., Ge, Z.-J., Zhang, C.-H. et al. (2011). Spindle assembly checkpoint regulates

mitotic cell cycle progression during preimplantation embryo development. *PLoS One* **6**, e21557. doi:10.1371/journal.pone.0021557

Wong, C. C., Loewke, K. E., Bossert, N. L., Behr, B., De Jonge, C. J., Baer, T. M. and Reijo Pera, R. A. (2010). Non-invasive imaging of human embryos before embryonic genome activation predicts development to the blastocyst stage. *Nat. Biotechnol.* **28**, 1115-1121. doi:10.1038/nbt.1686

Yao, T., Suzuki, R., Furuta, N., Suzuki, Y., Kabe, K., Tokoro, M., Sugawara, A., Yajima, A., Nagasawa, T., Matoba, S. et al. (2018). Live-cell imaging of nuclear-chromosomal dynamics in bovine in vitro fertilised embryos. *Sci. Rep.* **8**, 7460. doi:10.1038/s41598-018-25698-w

Zhang, C.-Z., Spektor, A., Cornils, H., Francis, J. M., Jackson, E. K., Liu, S., Meyerson, M. and Pellman, D. (2015). Chromothripsis from DNA damage in micronuclei. *Nature* **522**, 179-184. doi:10.1038/nature14493

Zhou, B., Ho, S. S., Zhang, X., Pattni, R., Haraksingh, R. R. and Urban, A. E. (2018). Whole-genome sequencing analysis of CNV using low-coverage and paired-end strategies is efficient and outperforms array-based CNV analysis. *J. Med. Genet.* **55**, 735-743. doi:10.1136/jmedgenet-2018-105272

Zimin, A. V., Delcher, A. L., Florea, L., Kelley, D. R., Schatz, M. C., Puiu, D., Hanrahan, F., Pertea, G., Van Tassell, C. P., Sonstegard, T. S. et al. (2009). A whole-genome assembly of the domestic cow, Bos taurus. *Genome Biol.* **10**, R42. doi:10.1186/gb-2009-10-4-r42

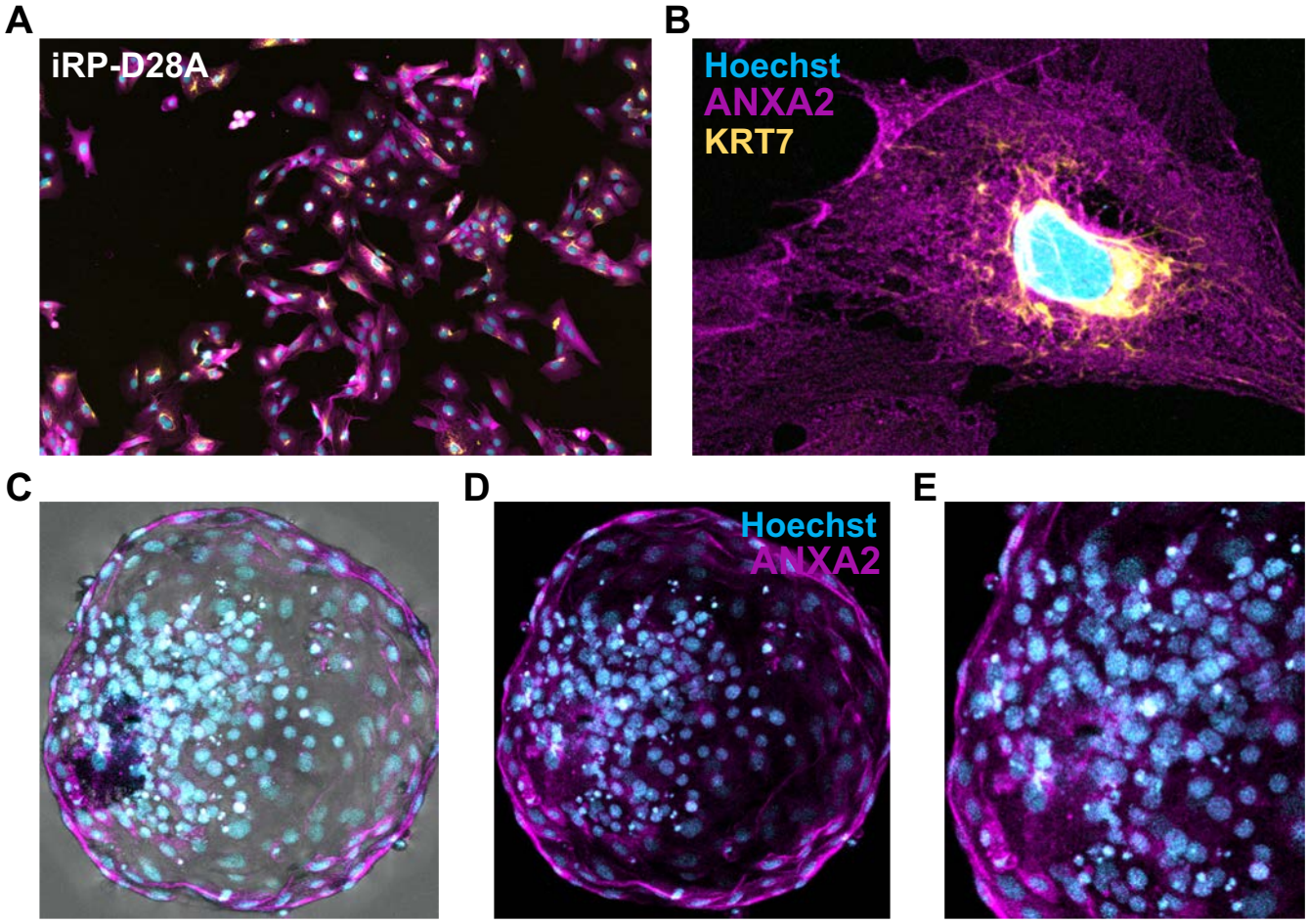

Fig. S1. Micronuclei are retained in either the TE or ICM of blastocysts. To confirm that micronuclei can be present in the TE or ICM of bovine blastocysts, we examined an additional TE marker, Annexin A2 (ANXA2), by immunofluorescence. **(A)** The specificity of the ANXA2 antibody was first tested in a highly-pure Day 28 immortalized rhesus placental (iRP) first trimester trophoblast cell line, iRP-D28A (Rosenkrantz et al. 2021), by staining the nuclei with Hoechst (blue) and immunolabeling with Cytokeratin-7 (KRT7), a pan-trophoblast marker. **(B)** Robust ANXA2 (pink) expression was observed in the iRP-D28A cells that co-localized with KRT7 expression (yellow). **(C)** Maximum intensity projection (MIP) confocal images of bovine blastocysts with clear separation of the TE and ICM and stained with Hoechst revealed multiple nuclear structures resembling micronuclei (10X). **(D)** Several of these micronuclei were contained within the ICM and negative for ANXA2 expression, **(E)** which was more apparent at higher magnification (20X).

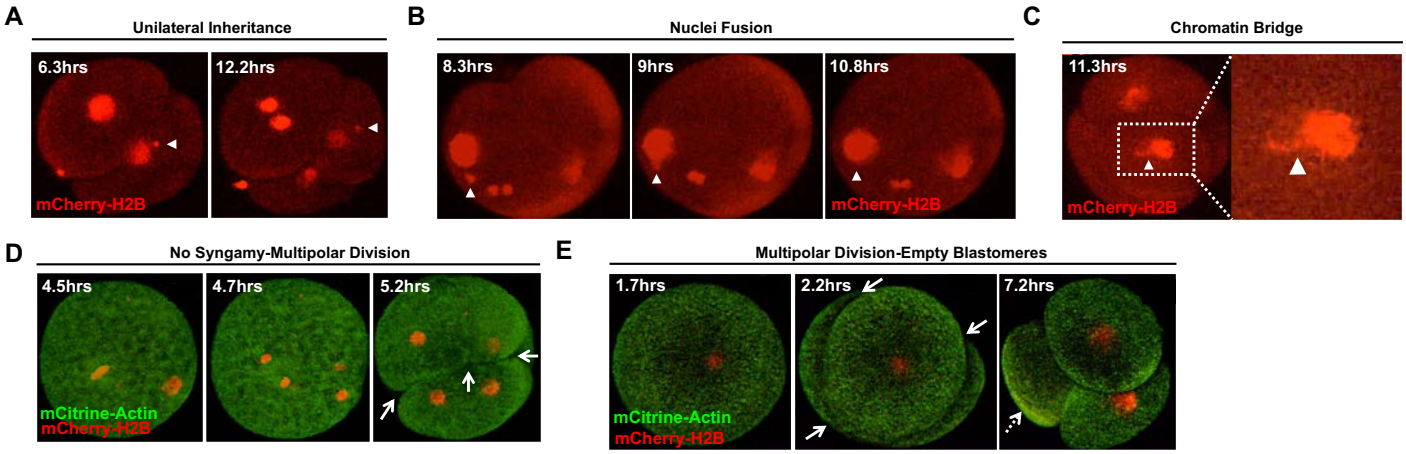

Fig. S2. Additional live-cell images representative of embryos with different phenotypes. Live-cell confocal microscopy of bovine zygotes microinjected with fluorescently labeled modified mRNAs to visualize DNA (Histone H2B-mCherry; red) and distinguish blastomeres (Actin-mCitrine; green) during the first three mitotic divisions. **(A)** Examples of other embryos with micronuclei that undergo unilateral inheritance, **(B)** fuse back with the primary nucleus, or **(C)** form a chromatin bridge (white arrowheads). **(D)** Images of additional embryos that bypassed pronuclear fusion (syngamy) prior to a multipolar division (white solid arrows) to produce blastomeres with asymmetric genome partitioning and/or **(E)** no apparent nuclear structure (white dashed arrows). Individual frames are represented in hours (hrs) from the start of imaging.

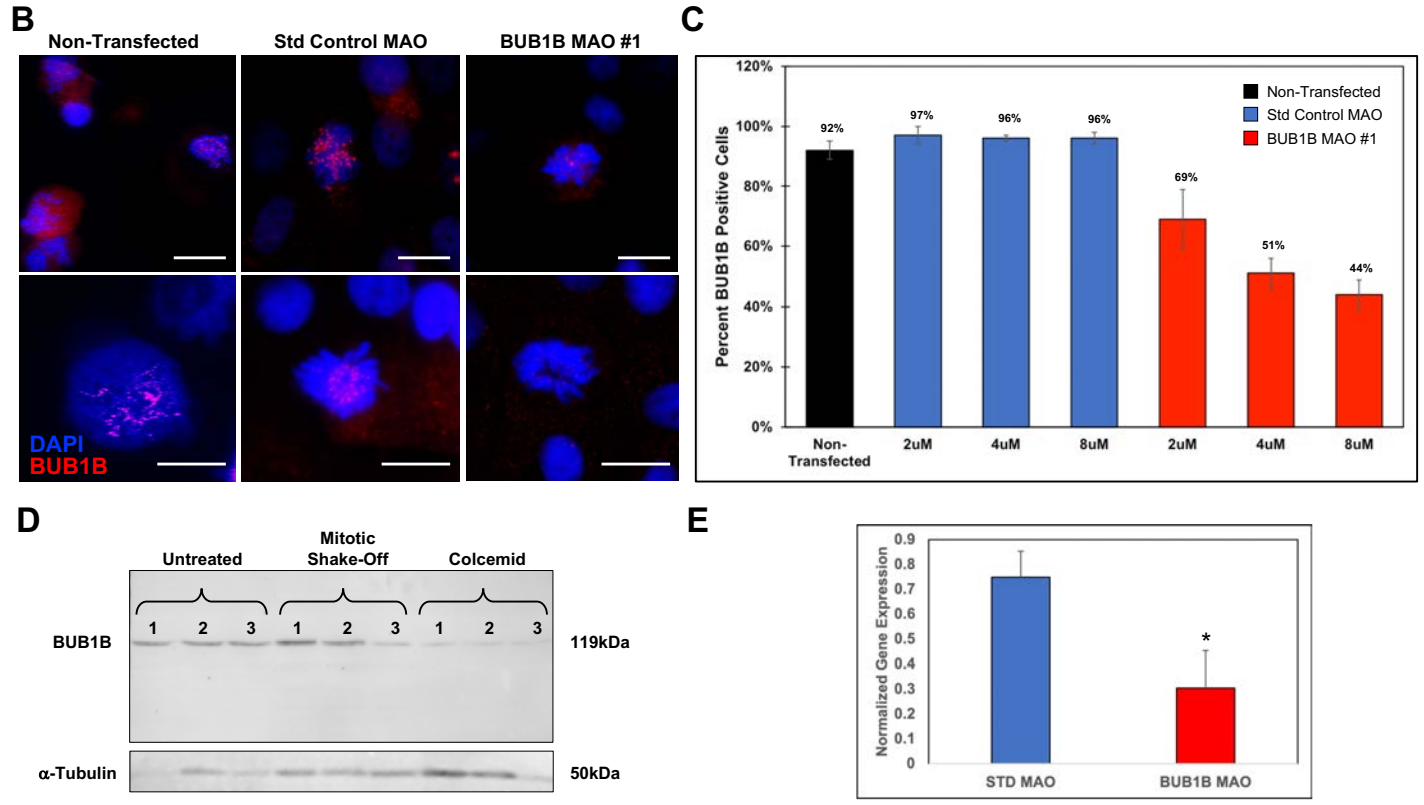

Fig. S3. BUB1B MAO design and knockdown efficiency. (A) DNA sequences of two non-overlapping MAOs designed to target the ATG start site (shown in red, BUB1B MAO #1) and the 5' UTR (depicted in blue, BUB1B MAO #2) of BUB1B. **(B)** BUB1B knockdown efficiency was assessed in synchronized MDBK cells following 48 hours of treatment with 3µl/ml of colcemid alone (non-transfected), the Std control MAO, or BUB1B MAO #1 via immunofluorescence. BUB1B protein expression was analyzed in DAPI stained (blue) MDBK cells. Note the lack of or reduced number of BUB1B positive foci (red) in the BUB1B MAO #1 treated cells compared to the controls; Scale bars = 10µm (top) and = 20µm (bottom). **(C)** Bar graph showing the percentage of MDBK cells in metaphase with BUB1B expression after colcemid treatment (black) or transfection with different concentrations (2, 4, and 8 µM) of the Std control MAO (blue) or BUB1B MAO #1 (red). While the number of cells exhibiting BUB1B positive foci was similar between the non-transfected and Std MAO controls, a dose-dependent significant decrease ($p<0.05$) in BUB1B expression was observed following BUB1B MAO #1 treatment using the Generalized Estimating Equations approach and Tukey's test for multiple comparisons. **(D)** Western Blot of BUB1B and α-Tubulin expression in untreated MDBK cells and following either mitotic shake-off or colcemid treatment all in triplicate to confirm reduced BUB1B expression at the protein level. **(E)** Quantitative RT-PCR (RT-qPCR) of normalized *BUB1B* expression in STD Control MAO versus BUB1B MAO injected bovine zygotes showing efficient BUB1B knockdown likely from negative feedback of inhibiting *BUB1B* mRNA translation. Mean CNRQ values ± SEM were compared using the Mann-Whitney U-test; *p=0.007.

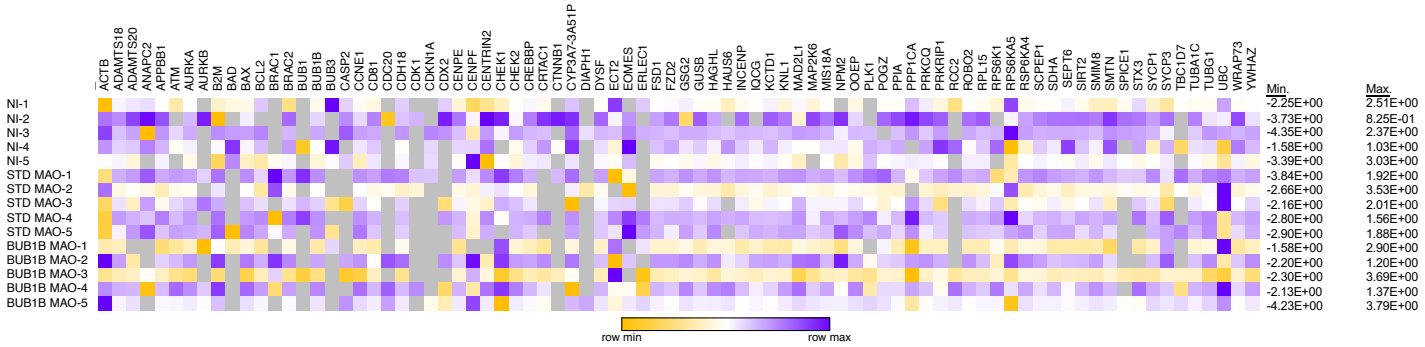

Fig. S4. Comprehensive assessment map of mitotic, of gene expression patterns in embryos. Heat cell cycle, developmentally-regulated, and cell survival genes assessed in individual BUB1B MAO #1 versus non-injected and Std Control-injected MAO bovine zygotes via single-cell microfluidic RT-qPCR. Cycle threshold (Ct) values were normalized to the most stable reference genes (*RPL15* and *GUSB*) across embryo groups and presented as the average. Gray squares indicated no expression, whereas yellow, white, and purple squares correspond to low, medium, and high expression, respectively. The range of expression levels for each gene with the minimum (Min.) and maximum (Max.) values is shown to the right of the heat map.

Table S1. Sequencing statistics of all embryonic and control samples. A table depicting the number or percentage of reads following de-multiplexing of embryonic (with embryo stage) and fibroblast samples at each step of the post-sequencing process, including adaptor removal, repeat masking, genome mapping, and quality assessment. The sequencing kit used and whether single- or paired-end is also included.

Click here to download Table S1

Table S2. List of all genes with primers analyzed by RT-qPCR in zygotes. A table of the genes analyzed by microfluidic qRT-PCR in non -injected bovine zygotes and following Std Control MAO versus BUB1B MAO #1 microinjection. Included is the sequence of the forward and reverse primer used for amplification as well as the NCBI accession number of each gene.

Gene Symbol	Forward primer sequence (5'->3')	Reverse primer sequence (5'->3')	NCBI Accession #
ACTB	CCTTCCTGGGCATGGAATCCT	GGCTTTTGGGAAGGCAAAGG	NM_173979.3
ADAMTS18	GCAGCGGATTAAACCACGATTA	ATCGGTAATGCAGGGAGCTG	NM_001192486
ADAMTS20	CAGGCAGGAAGCCTTAGTGA	TCTGTGGGAATACTTCGCCG	NM_001206093
ANAPC10	AACAGATTCCCCTTGCGGAG	CCACCAATTCAAGTTGCCGA	NM_001080357.2
ANAPC2	GTATTTCCAGGACCAAGCCAGC	GCGGCTCAGCCACAACTCT	XM_003584964.2
APPBB1	GATGAGACGCTGAAGCTGGT	ACGTAGGCAAAGTCCCTTCC	NM_001075186
ATM	GCCAGAATGTGAGCAACACC	AGCCAAGAACACCCACCAAA	NM_001205935.1
AURKA	AGCATGGATGAGTGGGTGAAT	TCTGTCCATGATGCCTGAGTC	NM_001038028.1
AURKB	TCCGACCCCTTACTCTCTCTC	AGGAACGCTTTGGGATGTTG	NM_183084.2
B2M	GCACCATCGAGATTTGAACATT	GCAGAAGACACCCAGATGTTG	NM_173893
BAD	TCAGGGGCCTCATTATCGGG	GGAAGCCCCTTGAAGGAGACG	NM_001035459.1
BAX	TAACATGGAGCTGCAGAGGATGA	CAGCAGCCGCTCTCGAA	NM_173894.1
BCL2	GAGGCTGGGACGCCTTTGT	GGCTTCACTTATGGCCCAGAT	NM_001166486.1
BRCA1	CCTACCTTGCAGGAAACCAGT	AATTGGTCTTGGCCTTGGCT	NM_178573.1
BRCA2	AGTTTCCGCTGTCTTCTCCC	GGTTTCTGTCGCCTTTGCAG	XM_002684277.2
BUB1	GCAGCTGGTGATAAAGGGGAA	AAAACTCCGATTCTCCGCGA	NM_001102011.2
BUB1B	AGCTACAAGGGCGATGACC	CTTTGTTCCCCTTTATCACCAGC	NM_001145173.1
BUB3	ATGGGACCACGCTTGCAATA	TGGTTAGGTGGACTTGGGTT	NM_001076177.1
CASP2	CTGTAGTCCCGCCGTTGAG	CATCGCTCTCCTCGCATTTG	NM_001144104.1
CASP3	ACGAAAATACTGGCATGGCCT	TCCGTTCTTTGCATTTCGCC	NM_001077840.1
CCNA1	CCTCACCTCTTACCCCCAGA	GCTTACTGCTCTGGTTGGAGT	XM_005194120.1
CCND1	AGATGTGACCCGGACTGCC	GGAAAACACCAGGACAGTGAG	NM_001046273.2
CCNE1	TTGCTGCTTCCGCCTTGTAT	TTGCTTGGGCTTTGTCCAGC	NM_001192776.1
CD81	ATTTCGTCTTCTGGCTGGCA	CGATAAGGATGTAGATGCCCACA	NM_001035099
CDC20	TGGAGCGGCGAGTTTAAGTT	CCATGGGAACGTCGTCAGT	NM_001082436.2
CDH18	AATGAAGATAACACAGCCAGCA	TGCTGAGAGAGGGGATTCCA	NM_001076837
CDK1	GCGGATAAAGCCGGGGTCT	GCTCTGGCAAGGCCAAAATC	NM_174016.2
CDK2	ATACACTGCGTTCCATCCCG	TACCACAGAGTCACCACCTCG	NM_001014934.1
CDKN1A	GGAGACCGTGGTTGGGAGA	CGTTTGGAGTGGTAGAAATCTGT	NM_001098958.2
CDX2	ACGTGAGCATGTATCCCAGC	TTCCTTTGCTCTGCGGTTCT	NM_001206299.1
CENPE	CCGTGGAGGTTTCTGACGTA	CAGGCGCTTCTTCTCTGTGA	XM_010805939.3
CENPF	CCTATTGCGGGAAAAAGAGCA	CTCGTTTAGCTTTAGCTCTTTCAG	NM_001256586.1
CENTRIN2	CGTCCGGGATGGCCTCTAA	AATGGCAGGCACTAAACCGA	NM_001038515.1
CHEK1	CAACTTATGGCAGGGGTGGT	ATGTAGCAGAGCTAGAGGAGC	NM_001098023.1
CHEK2	GGGTTTATCGCCACTCCGCT	ACCCATTTCTCTGAAGATCCGAAA	NM_001034531.1
CREBBP	CAAACTGGAGGGCAGCAGAT	CATCTGAGGCATGTTTGGCA	NM_001164022.1
CRTAC1	GACAAGCCCGTGTGTGTCAA	AAGGAGTGAGGGAGGCCACA	NM_001205325
CSPP1	TCCCTTCCTATTGGTGAGAGGT	GTCTGTTCCCGTACATCCTGTT	NM_001193015.2
CTNNB1	AGAACACAAATGACGTGGAGA	GACCTTCCATCCCTTCCTGTT	NM_001076141.1
CYP3A7-3A51P	GGCCATGGAGCTAATCCTGA	TCCATATAGATAGAGGAGCACCAGA	NM_001099367
DIAPH1	CACTAGCAACGCAAACCTGG	TTGAGGGAGACACGAAGGGA	XM_001787599.3
DYSF	ATGTGGGTCGACCTGTTTCC	CGCAGGAAAAACCTTCTGGC	NM_001102490
ECT2	ACGAGAGACAGAAGATTGCCA	GAGTATGTGAACCAAGAACCCA	NM_001097573.1
EOMES	GACAACTATGATTCATCCCATCAGA	TGATGGATGGGGGTGTCTCT	NM_001191188.1
ERLEC1	GCCAGTCACTACCAGGATCG	CCACCAACCAACACCCTCTT	NM_001191407.1
FSD1	AAGCTCAAGTTGGAACGGCT	CCAGCGCTTGAACCCATTAC	NM_001081518
FZD2	TCCACGGAGAGAAGGGCATA	CCCAGAAGGTTGGGCATGAT	XM_003587455.5
GSG2	ACAACAACTGCTGGGGTGAA	CTTCAAGGCGGGGGTGTTAT	NM_001076544
GUSB	TCCGCAGGGACAAGAATCAC	TGGGCAATCAGCGTCTTGAA	NM_001083436
HAGHL	CTGCCCCCTGAGACAAAGG	TGGTCGTTGTAAGGCTCCAC	NM_001075540
HAUS6	AGGTATCAAATGGTGATTTTGGCA	ATGCCACTGTGCATAGGACT	XM_002689566.6
INCENP	AGAACGCCTTCGCAGAAGAA	GTCTTTCTGCGGGACAACCT	XM_584352.7
IQCG	CGACCTACGCTTCGAGTACC	GGCTTCCAGACCTTCTTCCA	NM_001038195
KAT2A	TGTGAGCACCCTTTGGCTGA	AACGAGCCTTACTTGGGGAAG	XM_001788901.3
KAT2B	TTCGGGTGGGAAGGTTTCTG	TTCTGGTCAGCAGGCTTGAG	XM_613744.7
KCTD1	AATGGGCACAGAAGCAGCAA	ATATTGGGCCGACTGTCCTGG	NM_001080360
KNL1	CGGCGAGTAACTTTCGTCCT	AAACTTTTCTGAGCCCAGCG	XM_002690821.6
MAD2L1	GAGAGGTCCTTGAAAGATGGCA	AGACTTTTCTCTGGGTGCACTAT	NM_001191513.1
MAP2K6	TTGCATGAAGATTGCACGCC	TCGCTTCTTGCCTTTCGACT	NM_001034045
MCL1	CGGTGATTGGCGGAAGCG	AACCCATCCCAGCCTCTTTGTT	NM_001099206.1
MIS18A	TGCATCTTGCTACGCTGTGT	GTTGAGCGAACATCCTGTGC	NM_001098010
MYH2	AAGAGCCCTTGGAATGAGGC	GCTGAACTCAGAGGTCCTTGT	NM_001166227
NANOG	CGGACACTGTCTCTCCTCTTC	CCATTGCTATTCCTCGGCCA	NM_001025344.1
NPM2	GTGCTGTTGCTCAGTACGATT	ATGGTGTCTTACTGCCTCTTC	NM_001168706.1
OOEP	CGCCCGAGCTGAGAAAATGG	GGTGGGGAAAGGCAGAGATT	NM_001077869.2
PLK1	GTATGGCCTCGGGTATCAGC	TCGCGCTCGATGTACTGTAG	NM_001038173.2
POGZ	ACTACTACAGCTGGCAATTCTT	ATGGGCGAGGTCACTAGTTTG	NM_001163190.1
PPIA	GGATTTATGTGCCAGGGTGGTGA	CCAGGACCTGTATGCTTCAAAATG	NM_178320.2
PPP1CA	TGCCAAGAGACAGTTGGTGA	TGCCCATACTTGCCCTTATTCT	NM_001035316.2
PRKCQ	CCCAACCTTCTGTGAGCACT	CATTCATGCCACATGCGTCG	NM_001192077
PRKRIP1	AGAACTGGCTGCACTCCCA	GCAGTCAGCTCCTCCACATC	NM_001079641
RCC2	CTCCTCATCACCACGGAAGG	CAGGACCAGCGTGTGGTTAG	NM_001101911.2
ROBO2	ACAGATGATCTTCCACCACCAC	AAGTTGGCTGCTTGCTGTCT	XM_024993907.1
RPL15	GGCAGCCATCAGGGTGAG	CATCACGTCCGACTGCTTCT	NM_001077866.1
RPS6K1	GTTTCAGACACAGCCAAGGACC	ACAGAGCGCCCTTGAGTGAC	NM_001083722.1
RPS6KA5	ACCCCTTCTTCCAGGGTCTG	CAGGCTCCAGTCGGGTAAAT	NM_001192023.1
RSP6KA4	CACTCTTCACTACGCTGCCC	TTGTTGAAGGCGTGGAAAGTG	NM_001191400.1
SCPEP1	ACACATGGTTCCTTCCGACC	CAGCCCAGGCCATCCTATTC	NM_001045909
SDHA	TCCTGCAGACCCGGAGATAA	TCTGCATGTTGAGTCGCAGT	NM_174178
SEPT6	CCGATATAGCTCGCCAGGTG	CCAAACCTGTCTCTCCCACG	NM_001035430
SIRT2	GTCACGGGATAGAGCAGTCG	TCTGAGTCCTGAGCCTCCTG	NM_001113531.1
SMIM8	GCCTTTAAAAAGGAGCCGCC	AAGCCATTACAGGTTTGTTAGGT	NM_001081531
SMTN	GTTCTACCGCTGTCTGGTCC	CAGTCCACCAGCATCCGTG	NM_001076879
SPICE1	GCTATCGGGAAACGACAAGATGT	CGCCTGCGAGGAAAATCAAC	NM_001038117.2
STX3	TTTAGCAACTGAGCGAACAGG	CATACCCTCATCCCCTCTGC	NM_001101971
SYCP1	CCCGCCTTTTCCGAGTAGAT	TCCTCCCGAAGTCTGAGGTT	XM_003581953.2
SYCP3	CCAACAAGAGCAAAGGCAGAAG	TGCTGCTGTTACATGAGAGAAGAT	NM_001040588.2
SYT1	GACCATGAAAGATCAGGCCC	CAGCAGCTGGTTATTCTGGA	NM_174192
SYT2	CTTGCGGCAAAGACACTCC	CAGAGGGACAGCGGGGT	XM_024976596.1
TBC1D7	CGGACTTGGCCTAGGACTC	CAACTCCACGAAACCCCACT	NM_001015643
TEX14	ACGAAGTCCTGAAGGCGAAC	GATGGCTTCTACGAGTTCTTTCG	NM_001192568.1
TUBA1C	TTCTCCCCCGGACTCCTTAG	ATGCACTCACGCATAACGGA	NM_001034204
TUBG1	ACCAGCATCTCCTCGCTCTTT	CAGTAAGGCAGATGAGGGTCC	XM_001790429.3
UBC	GTCCGGACCGGGAGTTC	TCACAAAGATCTGCATTGTCAATTA	NM_001206307.1
WRAP73	GTACCTGGCTTCCTGCATCC	CACTCGAGGTGCTGGATCTG	NM_001193006
YWHAZ	ACCTACTCCGGACACAGAACA	ATCATATCGCTCAGCCTGCTC	NM_174814

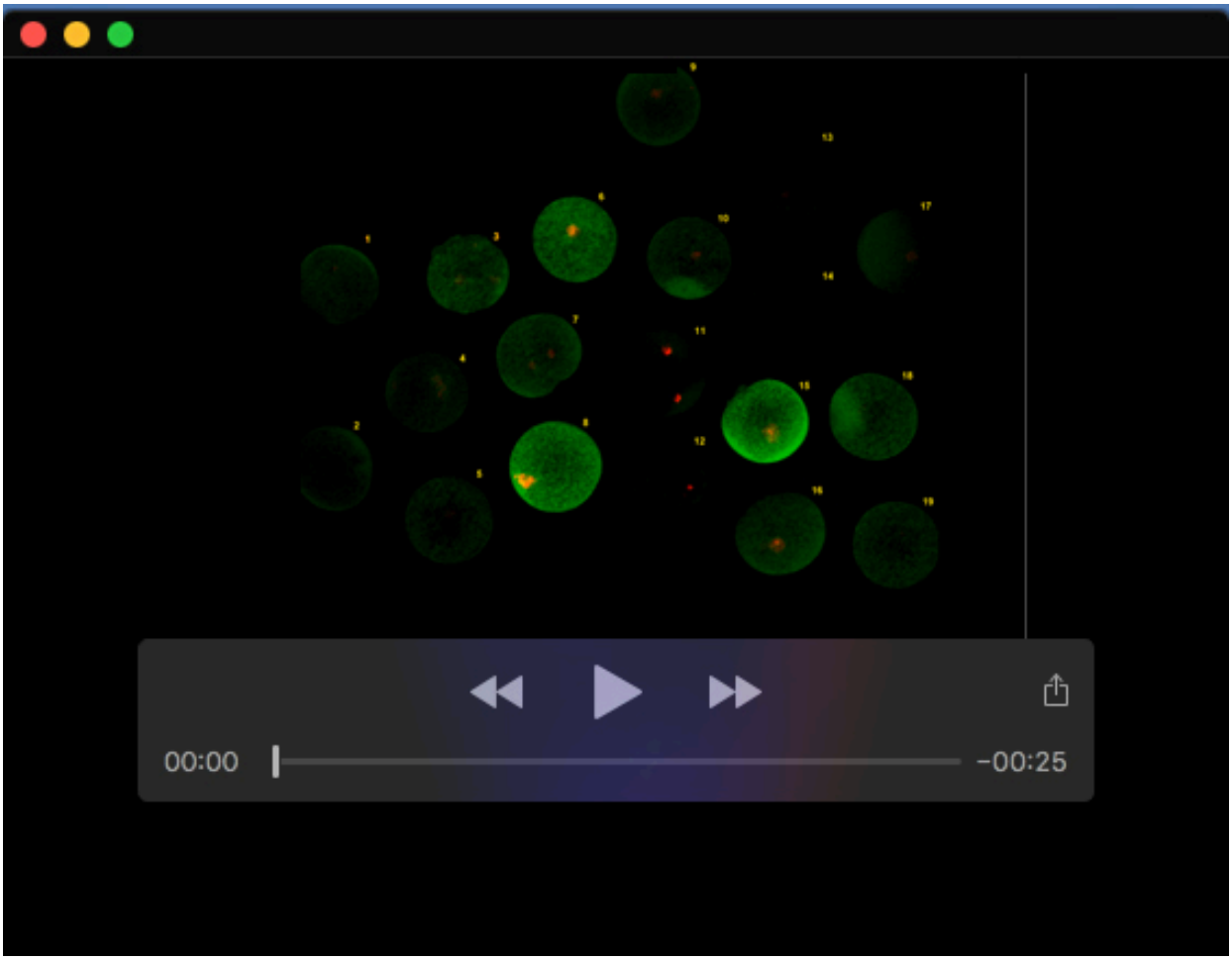

Movie 1. Live-cell fluorescent imaging of early cleavage divisions. Bovine zygotes were microinjected with fluorescently labeled modified mRNAs to mCitrine-Actin (green) and mCherry-Histone H2B (red) to distinguish blastomeres and DNA, respectively, and early mitotic divisions visualized by live-cell confocal microscopy. Note the micro-/multi-nuclei in embryos #3, #4, and #11, chromatin bridge in embryo #1, lack of syngamy in embryos #3 and #11, multipolar divisions in embryos #1, #3-6, #11, and #15, and production of empty blastomeres in embryos #5 and #15.

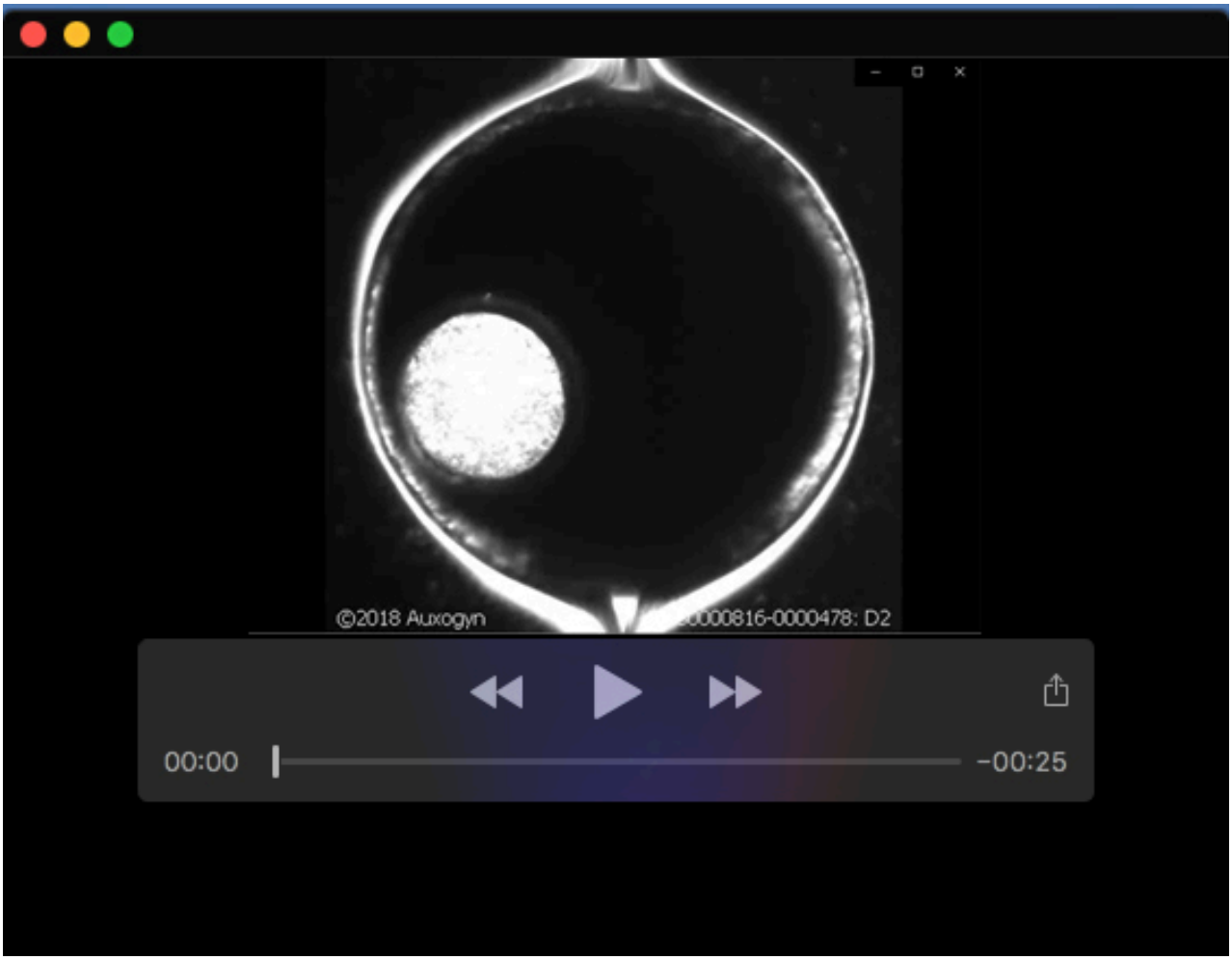

Movie 2. MCC-deficient embryos struggle to divide. A bovine zygote following BUB1B MAO microinjection attempted to divide by forming multiple cleavage furrows, but never successfully completed cytokinesis.

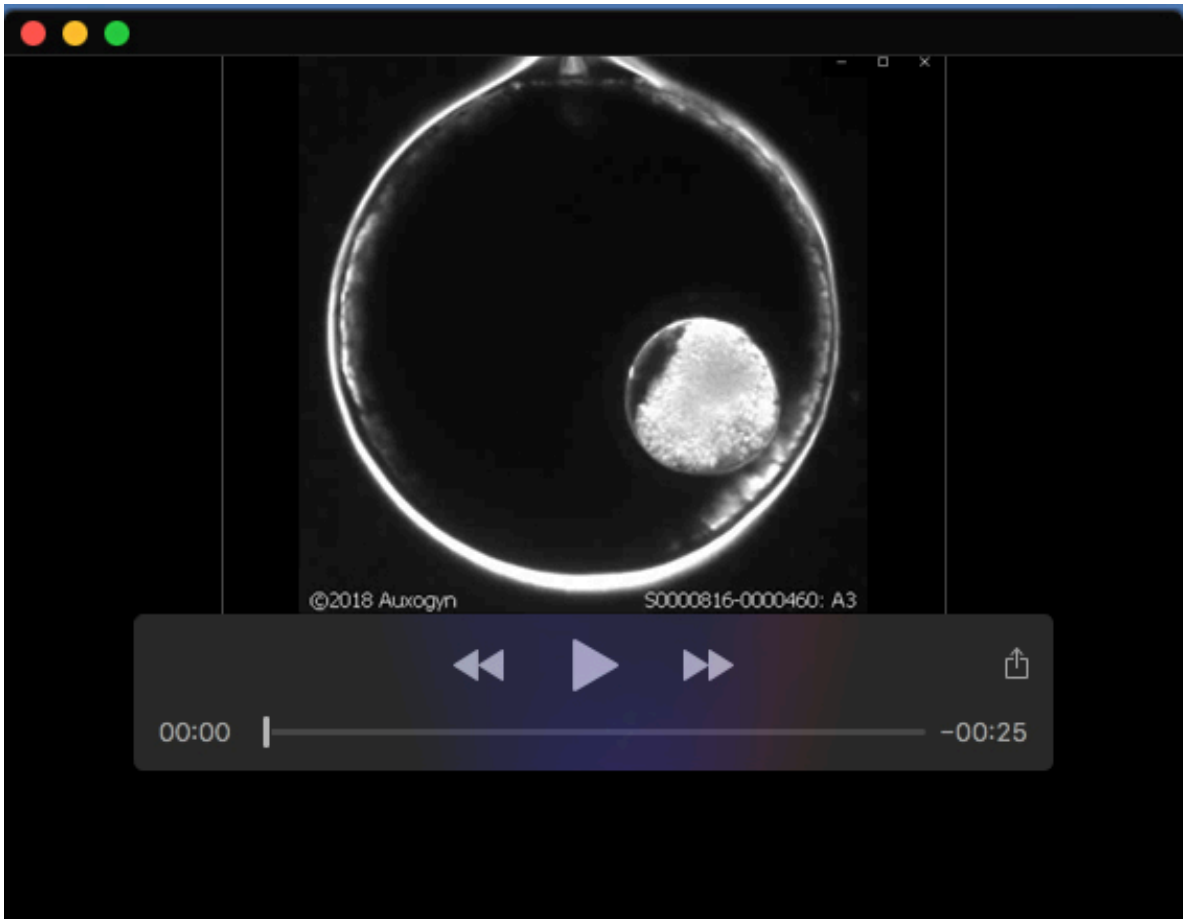

Movie 3. Multipolar divisions are observed in MCC-deficient embryos. Certain bovine zygotes were able to undergo cytokinesis even with BUB1B knockdown, but these divisions were abnormal with multipolar cleavage.

Movie 4. MCC deficiency causes blastomere asymmetry. Besides abnormal divisions, BUB1B-injected bovine embryos often exhibited blastomere asymmetry following the multipolar cleavage.